Journal of Applied Physics

RESEARCH ARTICLE | FEBRUARY 20 2024

Thermoelastic modeling of cubic lattices from granular materials to atomic crystals

Byung-Wook Kim ; Chao Liu ; Huiming Yin

J. Appl. Phys. 135, 075105 (2024)
https://doi.org/10.1063/5.0184120

Journal of Applied Physics ARTICLE pubs.aip.org/aip/jap

Thermoelastic modeling of cubic lattices from granular materials to atomic crystals

Cite as: J. Appl. Phys. **135**, 075105 (2024); doi: 10.1063/5.0184120
Submitted: 25 October 2023 · Accepted: 23 January 2024 ·
Published Online: 20 February 2024

View Online Export Citation CrossMark

Byung-Wook Kim, Chao Liu, and Huiming Yin[a)]

AFFILIATIONS

Department of Civil Engineering and Engineering Mechanics, Columbia University, 610 Seeley W. Mudd, 500 West 120th Street, New York 10027, New York, USA

[a)]**Author to whom correspondence should be addressed:** yin@civil.columbia.edu. **Tel.:** +1 212 851 1648. **Fax:** +1 212 854 6267

ABSTRACT

When a cubic lattice is confined by a surface layer, the effective thermoelastic properties can be tailored by the prestress produced by the surface. The thermal expansion coefficient, temperature derivative of elasticity, and the equation of state (EOS) of the solid depend on the potential of each bond and the lattice structure, which can be predicted by the recently developed singum model. This paper first uses a granular lattice confined by a spherical shell to demonstrate singum modeling of the thermoelastic behavior of the cubic lattices and then extends it to atomic crystal lattices by considering the surface tension and long-range interactions. Given the elasticity and the EOS of a cubic crystal, the interatomic potential can be inversely derived. As the bond length changes with thermal expansion and pressure, the singum model predicts the temperature- and pressure-dependent elasticity. Using the orientational average, isotropic elastic constants can be obtained for polycrystals. The case study of copper (Cu) demonstrates the versatility of the model for different cubic lattices and predicts the experimental results of pressure- and temperature-dependent elasticity. The singum model is general for different lattice types and EOS forms and provides clear physical and mechanical meanings to correlate the interatomic potential, EOS, and elasticity in the closed-form formulation, which is very useful in engineering design and analysis of metal structural members in fire, geothermal, and space applications without the needs of large-scale numerical simulations.

I. INTRODUCTION

Most solid materials exhibit periodically distributed atoms in the three-dimensional (3D) crystal lattice structures with interatomic forces. A solid with a stable atom lattice exhibits a well-defined elasticity given a certain temperature, which can be characterized by various mechanical tests. The correlation between the interatomic force or potential and the effective elasticity has been investigated by the equivalence of the elastic energy and pair potentials.[1,2] Because the interactomic forces referred to the center–center lines between atoms cannot fill the 3D continuous space, the equivalence was setup under different assumptions, which often lead to empirical or semi-empirical models. For example, the bulk modulus has been described by the equation of state (EOS),[3–5] while other elastic constants are simulated by interatomic potentials.[6–8] Recently, it was reported that external pressure can generate dislocations that would change interatomic forces in the diamond crystal lattice, and the transformation of gold crystal lattice was also investigated under external thermal loading.[9–11] Therefore, the thermoelastic properties of crystal lattices can be related to the interatomic forces.

On the other hand, although molecular dynamics, density functional theory, and *ab initio* models have been used to model the effective elastic behavior of solids from the basic atomic systems,[3,12,13] it typically requires a number of parameters and high computational costs to reach an accurate and stable prediction. However, some discrepancies commonly exist depending on the algorithms and parameter settings. An explicit formulation between the elastic constants and the interatomic potential can provide convenience in engineering design and analysis. There exists a need to bridge the discrete atom system and the continuum mechanics with the balance of the computational costs and accuracy.[14] Particularly, a closed-form equation of elasticity will be of significant interest in material and structural design.

For example, a metal material exhibits different mechanical behavior at different pressures and temperatures. For geothermal applications, a metal pipe in a geothermal borehole well is subjected

to significant change of the temperature and pressure at different depths.[15,16] Its stiffness may change with the depth in the borehole due to temperature and pressure variations. If the interatomic potential can be accurately described, it is possible to predict the pressure-dependent thermoelastic properties in an analytical way, which can be used in the design and analysis of the heat exchange system. Similar needs also exist in deep foundation of infrastructure, oil well drilling and operation, and space shuttle structures,[17,18] which are subjected to a large range of pressure and temperature variations.

The recent work[19] of the singum model uses the Wigner–Seitz (WS) cell[20] of an atom in the crystal lattice as a continuum particle to represent the atom. This allows to simulate an atomic particle system with singular atomic forces using a fully connected continuum system with stresses. Although a point force shows strong singularity, which commonly leads to infinite displacement or stress, the isotropic stress–strain relationship was established with the aid of the Fermi energy for bulk modulus by stress homogenization over the surface and orientation.[8] While the two independent isotropic elastic constants can directly map to the two constants in the interatomic potential given the crystal lattice characteristics, the simple form of the Fermi energy still cannot capture the general pressure–volume relation over a large range of deformation and was proposed to be replaced by a polynomial form.[2,8] Thus, it cannot be generalized to cubic crystals because the singum potential with two constants cannot fit the three elastic constants.

However, the singum model does provide the exact solution for the lattices with short-range interactions. For an example of a physical truss system or granular materials, the bonds are represented by springs with a harmonic potential or Hertz's contact changing with particle's center–center distance, respectively.[17] The singum model caught the physics and mechanics of the force transfer through a lattice and indeed provided an explicit, analytical form of elasticity with prestress in terms of the asymmetric and anisotropic tensor for lattice materials including metamaterials and composites.[21,22] The improved singum model[23] extended the formulation from the infinitesimal deformation to finite deformation for a face-centered cubic (FCC) lattice using the thermodynamic equation of state (EOS). The EOS of solids provides much more accurate description of the volume or density change of solids under an increasing hydrostatic pressure over a large range[4,5] for the bulk modulus prediction. The Vinet EOS[4] and Murnaghan–Birch (MB) EOS[24] have been widely used in the literature for the high accuracy and concise form of equations, whereas the MB EOS exhibits advantages with more parameters to fit experimental data for tailorable accuracy of higher order EOS.[23]

This paper extends the recent work[17,23] to thermoelastic modeling of cubic crystals. The MB EOS is used to derive the interatomic potential for general cubic crystals with FCC, body-centered cubic (BCC), and simple cubic (SC) lattices. The long-range atomic interactions are taken into account similarly to the embedded energy.[3] Given the elastic constants and the crystal lattice characteristics with the EOS, we can predict the singum interatomic potential and, thus, the pressure-dependent elasticity with the stretch ratio of the bond length in a closed-form expression. Although the dynamic effect of the kinetic energy of atoms caused by temperature, which will be studied in future work, is not considered yet, using the bond length changing with pressure and temperature, we can predict the thermoelastic behavior given the thermal expansion coefficient. Particularly, most engineering structural metals exhibit isotropic properties with a polycrystalline structure. Orientational average[19,25,26] has been conducted, so that the two independent elastic constants of an isotropic metal can be determined by the interatomic potential for the single crystal.

In the remainder of the paper, Sec. II uses a granular lattice confined by a spherical shell to demonstrate the thermoelastic behavior of the cubic lattices with prestress and formulates the elasticity and EOS in terms of the Hertz's potential for FCC, BCC, and SC granular lattices. Section III extends the singum model from granular lattices to atomic crystal lattices by considering the surface tension and long-range interactions. Given the EOS and elastic constants of an atomic lattice, the interatomic potential can be inversely derived. Therefore, the three elastic constants can be correlated with EOS and the singum potential. For polycrystalline metals, the isotropic elastic constants can be obtained by the orientational average. Section IV demonstrates the applications of the singum model to common metals using copper as an example, applies the singum model for pressure- and temperature-dependent elastic modeling of the polycrystalline metals, and shows the versatile capability of the model with some numerical results in comparison to some available experimental data in the literature. The model has been applied to thermoelastic modeling of two other metals, namely, nickel and tungsten, in the supplementary material (SM).

II. THERMOELASTIC MODELING OF A GRANULAR LATTICE IN A SPHERICAL SHELL

In the recent paper,[17] tailorable thermoelastic behavior of a cubic lattice packaged by a boundary layer can be achieved by changing the prestress. Negative thermal expansion and positive temperature derivative of elastic modulus can be obtained by the material design and predicted by the recently developed singum model.[19] This section uses granular lattices to demonstrate the singum model and predict the effective thermoelastic behavior.

A. Overview of the singum model

Consider many small balls are filled in a large spherical shell as illustrated in Fig. 1. Assuming that all the balls are identical spheres with initial radius l_p^0, Young's modulus E^0, and Poisson's ratio ν^0, the contact force between particles changes with the center to center distance $2l_p$ following the Hertz's model can be

$$P = 4\gamma\left(l_p^0\right)^2(1-\lambda)^{3/2}, \tag{1}$$

where $\lambda = l_p/l_p^0$ is the stretch ratio and $\gamma = \frac{E^0}{3[1-(\nu^0)^2]}$.[27] The small balls are confined by a spherical shell with radius R, thickness t, Young's modulus E, and ν. Here, l_p^0, $t \ll R$. Although the cubic lattice of small balls cannot perfectly fill the spherical shell because the balls are so small, the boundary effect will be minimal, so that the lattice can still be treated as a continuum overall. To create prestress, the lattice of small balls is also in the form of large ball with radius R^0, but $R^0 > R$. The misfit will produce compressive force in the lattice and tension in the shell. When the effective elastic behavior of the lattice is given, we can predict the final radius of

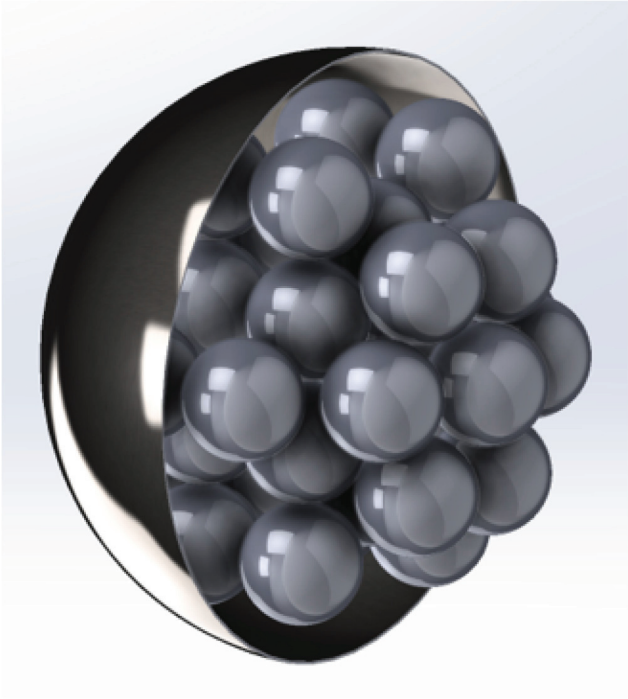

FIG. 1. Schematic illustration of a granular lattice of small balls confined in a spherical shell with prestress—the size of balls is enlarged for better visualization.

the lattice R and calculate the prestress in the lattice and the shell. Here, the stretch ratio of the bond can be defined as $\lambda = R/R^0$. When the composite consisting of multiple balls enclosed by the shell is subjected to a temperature change or a mechanical load, the effective thermoelastic behavior will change with the prestress and lattice structure.[17]

Given a cubic lattice in Fig. 2 with each center numbered as the 0th point to set up the singum particle, there are N closest particles as the singum members, where $N = 12, 8$, and 6 for FCC, BCC, and SC, respectively, in Figs. 2(a)–2(c). As the lines from the singum center to the other centers of the closest singums can be treated as bonds, the singum model transfers the singular forces and displacements of the bonds to the corresponding stress and strain of the singum volume for the effective thermoelastic properties at the continuum level.

Each singum particle can be constructed as the WS cell by enclosing surrounded planes, which is perpendicular to the bonds as well as intersecting at their halves with the surface norm $\mathbf{n}^I$, where $I = 1, 2, \ldots, N$. The bond length between the 0th point and any of the Nth points is initially $2l_p^0$ and the edge length of the conventional cubic unit cell is denoted by a^0, whereas $2l_p$ and a represent the actual bond length and edge length, respectively, under the prestressed state, so that the length change can also be represented by the stretch ratio $\lambda = l_p/l_p^0 = a/a^0$. As shown in Figs. 1(d)–1(f) for FCC, BCC, and SC, respectively, a Cartesian coordinate $\mathbf{X}$ is set up at the initial condition with bond length $2l_p^0$, i.e., the Lagrangian coordinates, while $\mathbf{x}$ are referred to the deformed state or the Eulerian coordinates, during a homogeneous deformation in which the lattice still maintains its periodic structure with planar surfaces of the singum. Thus, the initial singums or the deformed singums can completely fill the entire space without any of gaps or overlaps. Furthermore, due to the central symmetry of the lattice, the singum particles keep in equilibrium under the deformation, so that the origins of $\mathbf{x}$ and $\mathbf{X}$ are both selected at the 0th point without any loss of generality.

Since the lattice transfers force through the bonds between the neighboring singum particles, the singum model is formulated based on the following assumptions:

(1) The interaction between singum particles is governed by the interatomic potential $V(\lambda)$, where λ is the normalized interatomic distance or stretch ratio. At the zero-force bond length, $\lambda = 1$, the hydrostatic deformation can be described by the interatomic distance $2l_p = 2\lambda l_p^0$ or $\lambda = l_p/l_p^0$.
(2) The interaction between two neighboring singums is through the surface stress vector along their contact surface, whose resultant force is equivalent to their interatomic force, i.e., $F_j = \frac{V_\lambda}{2l_p^0} n_j$. Here, $\mathbf{F}$ and $\mathbf{n}$ denote the interatomic force and bond directional norm vector, respectively.
(3) The surface layer or spherical shell confines the boundary of the lattice and produce prestress to the singums, which is similar to surface tension to liquid balloon. Therefore, the force between singums can be tailored even when the undeformed lattice is free from the external loading.
(4) Only the contact force between singums is considered and the long-range interatomic force beyond the bond length is not directly considered, such as magnetic, electric, and gravitational forces. This assumption can be released in later discussion.

Based on Assumption 3, the zero-force state of the singum at bond length $2l_p^0$ in Fig. 2 shall be different from the undeformed state because the boundary layer produces a prestress, similar to surface tension, on the singum. Therefore, the undeformed state of the lattice with the bond length $2l_p^u$ can be indicated by $\mathbf{x}^u$. Note that the resultant force on a singum from all neighboring singums is still zero due to the symmetry of the forces, so that the singum can maintain equilibrium. In the following discussion, the initial state uses superscript 0 and the undeformed state superscript u.

B. Formulation of elasticity with Hertz's contact potential

Now at the initial state $\mathbf{X}$, the lattice is represented by a homogenous material consisting of singums, the mass conservation defines the density of the material as

$$\rho^0 = \frac{M_a}{v_s^0}, \tag{2}$$

where M_a is the mass of the ball and v_s^0 is the singum volume at the zero-force bond length $2l_p^0$ for cubic lattices as expressed in Table I.

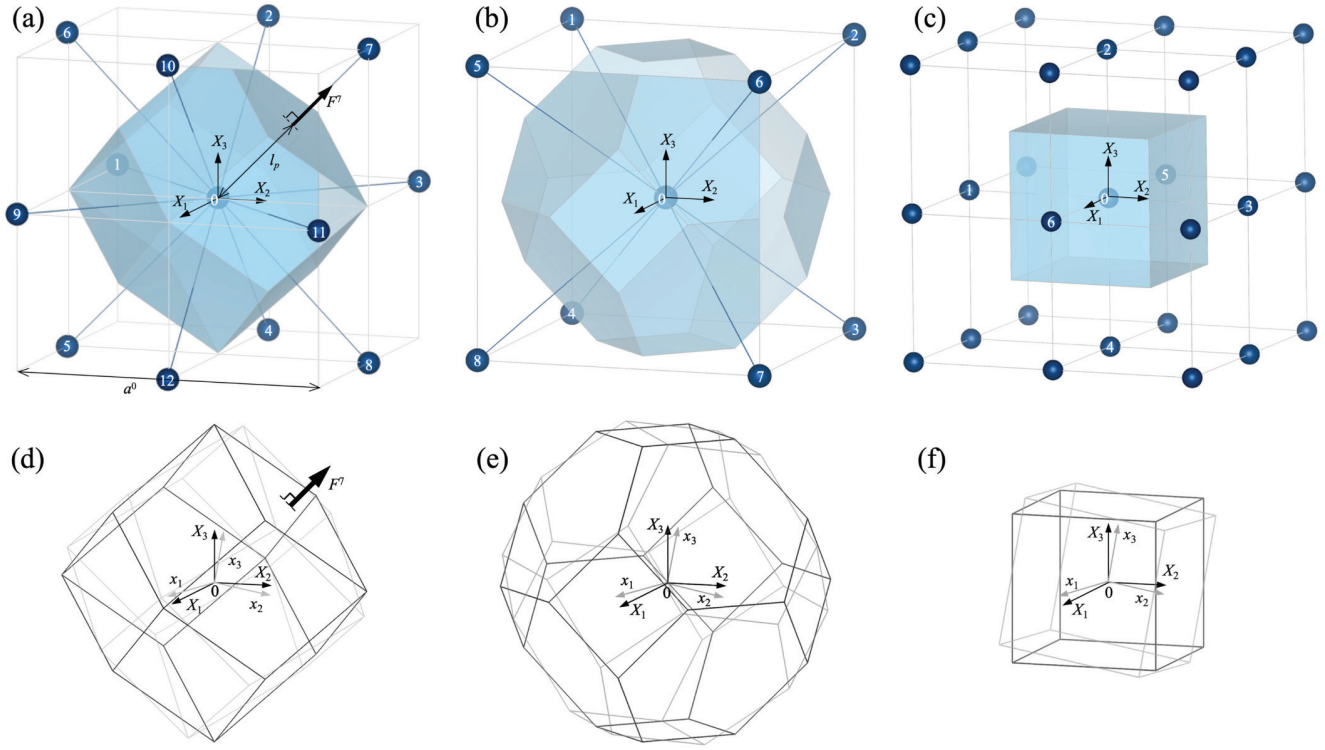

FIG. 2. The singum model of a cubic lattice: (a) an FCC lattice with a rhombic dodecahedron singum, (b) a BCC lattice with a truncated octahedral singum, (c) an SC lattice with a cubic singum, (d) FCC singum, (e) BCC singum, and (f) SC singum at the initial state with **X** and at the deformed state with **x**.

Since the potential of the singum particle V determines the mechanical properties of the lattice, the inter-particle force changing with the center–center distance can be calibrated with the experimental data, and various contact models have been studied to estimate the forces for the particle interactions. One such model, developed by Hertz in 1896,[28] assumes frictionless contact and linear elasticity under small strain conditions. When contact pressures exceed the material's yield strength, an elastic–plastic model is utilized,[29] taking into account energy dissipation. Considering both elasticity and viscosity effects, the Kuwabara and Kono model proves visco-elastic behaviors of particles.[29,30] For tiny particles, such as nanoparticles and powders, where adhesive forces cannot be neglected, the JKR (Johnson–Kendall–Roberts) and DMT (Derjaguin–Muller–Toporov) models are commonly applied to address adhesive interactions.[29,31–33] These models collectively provide a versatile framework for approximating the diverse forces governing particle interactions. While the singum model can utilize any of these empirical functions, the Hertz potential is employed with Eq. (1) for the singum particle interaction in this work.

TABLE I. The lattice parameters and bulk moduli for cubic lattices.

Lattice	FCC	BCC	SC
N	12	8	6
v_s^0	$4\sqrt{2}\left(l_p^0\right)^3$	$\frac{32\sqrt{3}\left(l_p^0\right)^3}{9}$	$8\left(l_p^0\right)^3$
$k=\frac{N(\lambda V_{\lambda\lambda}-2V_\lambda)}{18v_s^0}$	$\frac{\lambda V_{\lambda\lambda}-2V_\lambda}{6\sqrt{2}\left(l_p^0\right)^3}$	$\frac{\lambda V_{\lambda\lambda}-2V_\lambda}{8\sqrt{3}\left(l_p^0\right)^3}$	$\frac{\lambda V_{\lambda\lambda}-2V_\lambda}{24\left(l_p^0\right)^3}$

As the singum particle deforms, the stress in the continuum still satisfies the equilibrium equation in the absence of the body force or inertia force as

$$\sigma_{ij,i}=0, \tag{3}$$

where σ_{ij} is the stress tensor in a solid. The stress integral of the singum caused by the neighboring singums can be written as[23,34]

$$S_{ij}=\int_{v_s}\sigma_{ij}(\mathbf{x})d\mathbf{x}=\Sigma_{I=1}^{N}x_i^I F_j^I, \tag{4}$$

where x_i^I indicates the coordinate of the cutting point of the bond, and the inter-particle force can be written in terms of the derivative of the potential in Assumption 2. Although the stress cannot be well-defined on singum particles, it can be measured on the

singum through the average stress, namely, the singum stress,[21]

$$\sigma_{ij} = \frac{S_{ij}}{v_s} = \frac{\Sigma_{I=1}^{N} x_i^I F_j^I}{v_s}, \tag{5}$$

where $v_s = \lambda^3 v_s^0$ is the current volume of the singum and N is the number of the closest neighbors for each cubic lattice as tabulated in Table I, and the variation of average stress can be obtained by taking the variation of Eq. (5) as

$$\delta\sigma_{ij} = \frac{1}{v_s}\Sigma_{I=1}^{N}\left(x_i^I F_{j,k}^I \delta x_k + F_j^I \delta x_i^I - x_i^I F_j^I \frac{\delta v_s}{v_s}\right). \tag{6}$$

In addition to the stress, the singum strain is defined as the average displacement gradient tensor of the singum $\mathbf{u}^I$, related to the displacement of the cutting point of the bonds,

$$d_{ij} = \frac{\int_{V_s} u_{j,i} d\mathbf{x}}{V_s} = \frac{\int_{\partial V_s} n_i u_j d\mathbf{x}}{V_s} = \frac{\sum_{I=1}^{N} A^I n_i^I u_j^I}{V_s}, \tag{7}$$

where A^I, $\mathbf{n}^I$, and $\mathbf{u}^I$ are the area, out-norm, and displacement of each cutting surface or points of the singum.[21] Notice that for some lattices, the number of singum surfaces is higher than that of the bonds: for example, BCC's singum exhibits 14 surfaces and 8 bonds, so that the singum strain needs to be redefined according to each cutting surface with the displacement at its center in Eq. (7) instead of the cutting bonds. However, given a variation of singum strain δd_{ij} due to the periodicity of the lattice, the Cauchy–Born rule can be applied to each cutting point as

$$\delta u_j^I = x_i^I \delta d_{ij}. \tag{8}$$

For a displacement-controlled load, the singum strain is prescribed, so Eq. (8) shall be used and Eq. (7) becomes a reference only. The Eulerian strain variation caused by $\delta\mathbf{u}$ can be written as[23]

$$\delta\varepsilon_{ij} = \frac{\delta d_{ij} + \delta d_{ji}}{2\lambda^2}, \tag{9}$$

where the higher order term of δd_{ij} is disregarded as the strain variation is infinitesimal.

Therefore, with the obtained stress variation and strain variation, the stiffness tensor C_{ijkl} at the current state can be defined by the relationship between them as follows:

$$\delta\sigma_{ij} = C_{ijkl}\delta\varepsilon_{kl}. \tag{10}$$

Using $n_i^I = \frac{x_i^I}{|\mathbf{x}^I|} = \frac{x_i^I}{l_p}$ and writing the summation of $n_i^I n_j^I$ and $n_i^I n_j^I n_k^I n_l^I$ in terms of Kronecker Delta,[23] one can find that δd_{ij} and δd_{ji} produce the same stress state and, thus, obtain

$$C_{ijkl} = c_{12}\delta_{ij}\delta_{kl} + (c_{11} - c_{12} - 2c_{44})\delta_{IK}\delta_{ij}\delta_{kl} + c_{44}\left(\delta_{ik}\delta_{jl} + \delta_{jk}\delta_{il}\right), \tag{11}$$

where $c_{11} = C_{1111}$, $c_{12} = C_{1122}$, and $c_{44} = C_{1212}$ following the Voigt notation. They can be written in terms of the derivatives of $V(\lambda)$ for FCC, BCC, and SC, respectively, as follows:

$$\begin{aligned}
c_{11} &= \frac{\lambda V_{,\lambda\lambda} + V_{,\lambda}}{4\sqrt{2}l_p^{0^3}}; \quad \frac{\lambda V_{,\lambda\lambda} + 2V_{,\lambda}}{8\sqrt{3}l_p^{0^3}}; \quad \frac{\lambda V_{,\lambda\lambda}}{8l_p^{0^3}}, \\
c_{12} &= \frac{\lambda V_{,\lambda\lambda} - 5V_{,\lambda}}{8\sqrt{2}l_p^{0^3}}; \quad \frac{\lambda V_{,\lambda\lambda} - 4V_{,\lambda}}{8\sqrt{3}l_p^{0^3}}; \quad -\frac{V_{,\lambda}}{8l_p^{0^3}}, \\
c_{44} &= \frac{\lambda V_{,\lambda\lambda} + 3V_{,\lambda}}{8\sqrt{2}l_p^{0^3}}; \quad \frac{\lambda V_{,\lambda\lambda} + 2V_{,\lambda}}{8\sqrt{3}l_p^{0^3}}; \quad \frac{V_{,\lambda}}{8l_p^{0^3}}.
\end{aligned} \tag{12}$$

Here, Mura's extended index notation is used for $\delta_{IK}\delta_{ij}\delta_{kl}$ as follows:[34]

(1) Repeated lower case indices are summed up as usual index notation; and
(2) Uppercase indices take on the same numbers as the corresponding lower case ones but are not summed.

When multiple copper (Cu) balls in a thin spherical shell as shown in Fig. 1 are subjected to a hydrostatic external load p, if the thin shell produce a negligible resistance to the external load due to the small thickness or stiffness, the load is fully transferred to the granular lattice that is constructed by those balls with the periodicity. Due to the central symmetry, the lattice will exhibit a volume change while maintaining its lattice structure, which can be described by the stretch ratio λ with the bulk modulus k as plotted in Fig. 3(a),

$$k = \frac{2N\gamma\left(l_p^0\right)^3(1-\lambda)^{1/2}(4-\lambda)}{9v_s^0}, \tag{13}$$

where v_s^0 and N can be chosen for granular lattice structures from Table I. If the granular lattice is FCC, the equation of state (EOS) of the lattice, the relationship between pressure p and volume v_s, can be plotted as Fig. 3(b) and given by the singum model as

$$p = 4\gamma\left(l_p^0\right)^2(1-\lambda)^{3/2}, \tag{14}$$

where $\lambda = l_p/l_p^0 = \left(v_s/v_s^0\right)^{1/3}$, in which v_s is the singum volume at the corresponding pressure p, and the Hertz's potential is derived from Eq. (1) as

$$V = -2\int_1^\lambda P l_p^0 d\lambda = \frac{16}{5}\gamma\left(l_p^0\right)^3(1-\lambda)^{\frac{5}{2}}, \tag{15}$$

where it uses $V(0) = 0$ as the reference. Therefore, the derivatives of V can be obtained as

$$\begin{aligned}
V_{,\lambda}(\lambda) &= -8\gamma\left(l_p^0\right)^3(1-\lambda)^{\frac{3}{2}}, \\
V_{,\lambda\lambda}(\lambda) &= 12\gamma\left(l_p^0\right)^3(1-\lambda)^{\frac{1}{2}},
\end{aligned} \tag{16}$$

where $\gamma = \frac{E^0}{3[1-(\nu^0)^2]} = 47.37$ GPa with $E^0 = 124.7$ GPa and $\nu^0 = 0.35$ for Cu. Likewise, if the granular lattice is BCC or SC, one can also find its bulk modulus with the potentials using Table I.

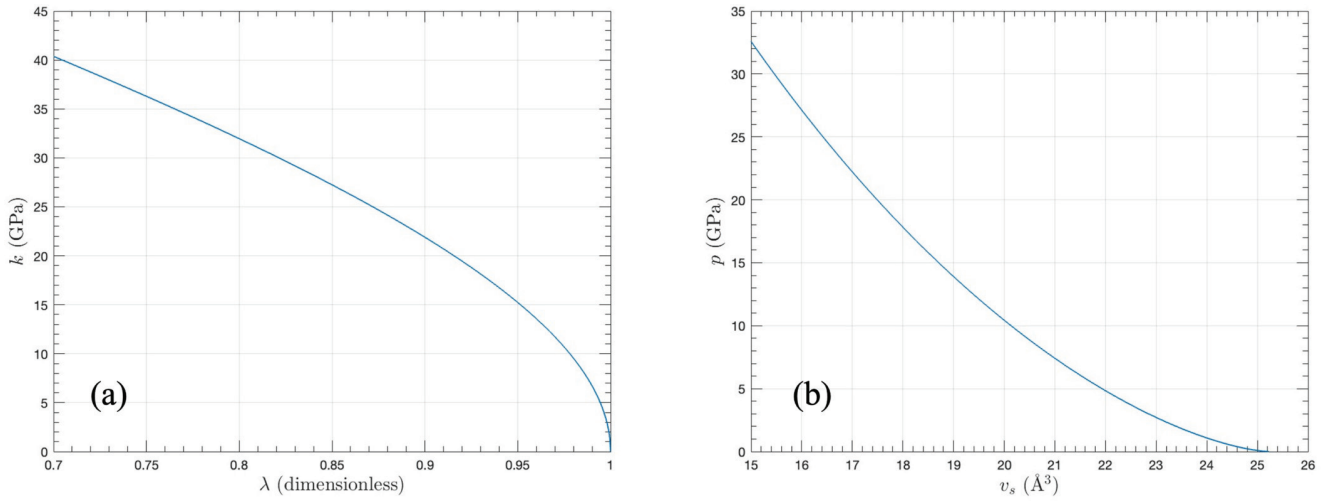

FIG. 3. Elastic behavior of granular Cu FCC lattice: (a) bulk modulus k as a function of λ; (b) hydrostatic pressure p as a function of the sigum volume v_s.

Note that the Hertz contact limits $\lambda \leq 1$ for compressive force only. For adhesion of particles, the Derjaguin–Muller–Togoroov (DMT) and Maugis models[32,35] provide the sticking force changing with the contact area. The adhesion force and force-separation law the those models can be used to enrich the potential function in the adhesion phase, so that the attraction force between particles can be considered. Therefore, a more versatile potential function $V(\lambda)$ can be used in Eq. (15) to cover the adhesion. Although the present paper used the Hertz potential only for granular materials, indeed, the formulation can be extended to any form of potential functions, including higher order contact models and common interatomic potentials.

C. The thermoelasticity of a copper shell filled with an FCC lattice

In general, when identical multiple materials are assembled to construct a certain structure without any stress, the structure exhibits the same thermal expansion coefficient of the constituent materials because it experiences an affine transformation with their same shapes. However, when a prestress is applied to the structure, the thermomechanical behaviors would change owing to the induced configurational stress induced. While the recent work demonstrated that it is possible to achieve zero or negative thermal expansion coefficient and positive temperature derivative of the elastic modulus for a spherical titanium shell filled with aluminum granular lattices using the prestress caused by the material misfit,[17] we consider a copper spherical shell having an internal radius R^s filled with identical copper balls forming a granular FCC lattice having an radius R^l: $R^s \leq R^l$. When the granular lattice is sealed by the shell, the inherent difference in their radii gives rise to a hydraulic prestress, denoted as σ^l, which can be quantified through the integration of the bulk modulus k of the granular lattice,

$$\sigma^l = 3\int_1^{\lambda} \frac{k(\lambda)}{\lambda} d\lambda. \tag{17}$$

Since the bulk moduli for cubic lattices are well defined in the singum model as expressed in Table I, the membrane stress on the shell σ^s is also obtained from the equilibrium condition,[17]

$$\sigma^s = -\frac{\sigma^l R}{2t} \tag{18}$$

where R is the final radius, and the membrane strain ε^s can be solved as

$$\varepsilon^s = \left(\frac{1-\nu^s}{E^s}\right)\sigma^s = \frac{R-R^s}{R}, \tag{19}$$

where ν^s and E^s are Poisson's ratio and Young's modulus for the shell. Given the initial radius at the initial temperature $R(T_0)$ and the final radius at different temperature $R(T_1)$, the effective thermal expansion coefficient α^{eff} of the prestressed granular lattice by the enclosed shell would be

$$\alpha^{eff} = \frac{R(T_1)-R(T_0)}{R(T_0)(T_1-T_0)}, \tag{20}$$

with the stretch ratio $\lambda = R(T_1)/R(T_0)$, and the effective temperature derivative of Young's modulus $E^{eff}_{,T}$ can be also obtained as

$$E^{eff}_{,T} = \frac{E(T_1)-E(T_0)}{T_1-T_0}. \tag{21}$$

where T_1 shall be very close to T_0 to obtain a convergent result.

Based on the previous discussion, we provide a case study to show the prestress effect on the effective thermal expansion coefficient for the composite consisting of multiple copper balls enclosed by a copper shell. Assuming that a small temperature variation is introduced, the material properties such as thermal expansion

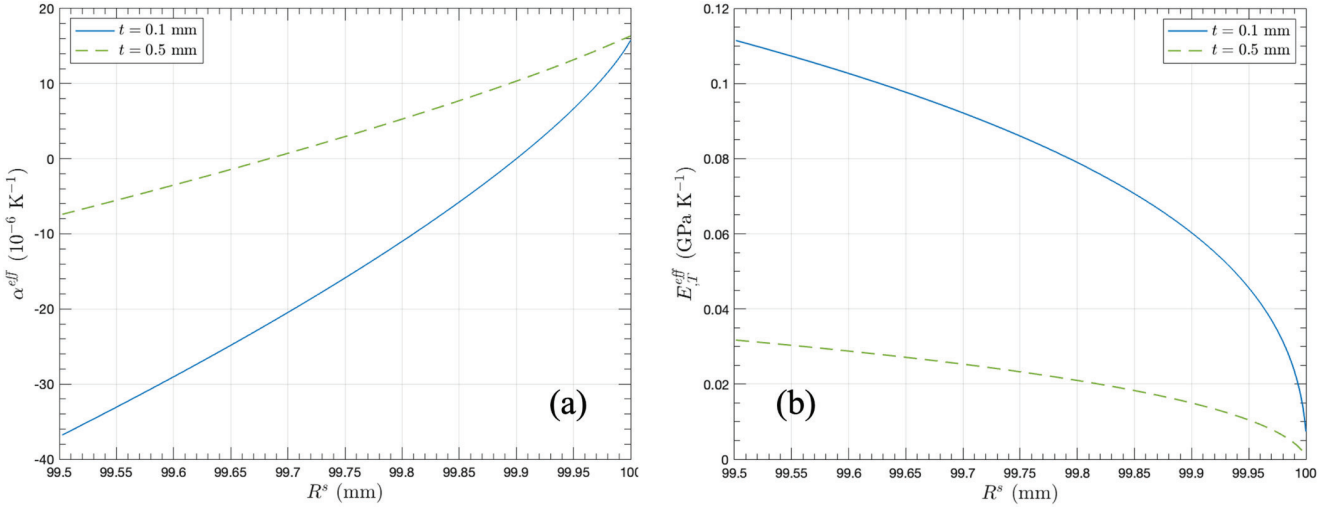

FIG. 4. Thermomechanical behavior of a copper granular lattice in a copper shell with prestress: (a) effective thermal expansion coefficient α^{eff} and (b) effective temperature derivative of Young's modulus $E_{,T}^{eff}$ as a function of internal radius of shell R^s with different shell thicknesses of $t = 0.1$ and 0.5 mm.

coefficient α, Young's modulus E, and Poisson's ratio ν are considered as constant around 300 K. When copper exhibits $\alpha = 16.61 \times 10^{-6}\,K^{-1}$ at 300 K with the internal radius of the shell $R^s = 100$ mm and the copper ball radius $l_p^0 = 5$ mm,[36] Figs. 4(a) and 4(b) show α^{eff} and $E_{,T}^{eff}$ in terms of R^s and t, respectively. Notice that the previous work[17] demonstrated similar behaviors with aluminum balls in a titanium shell.

If the internal radius of the shell is equal to the initial radius of the lattice: $R^s = R^l = 100$ mm or $\lambda = 1$, the effective thermal expansion coefficient α^{eff} converges to the intrinsic thermal expansion coefficient, $16.61 \times 10^{-6}\,K^{-1}$. However, as R^s decreases from the initial radius of 100 mm, α^{eff} approaches to zero at $R^s = 99.9$ and 99.7 mm for $t = 0.1$ and 0.5 mm, respectively, and even negative α^{eff} was shown with smaller R^s or further hydraulic prestress due to higher mismatch between the shell and the lattice radii. This represents that the prestress could significantly tailor material properties within 5% change of the lattice radius, and the tailorable range could be also chosen with t, as thinner t shows wider range of α^{eff}: $\alpha^{eff} = -36.78 \sim 16.61 \times 10^{-6}\,K^{-1}$ with $t = 0.1$ mm and $\alpha^{eff} = -7.40$–$16.61 \times 10^{-6}\,K^{-1}$ with $t = 0.5$ mm. The temperature derivative of Young's modulus also becomes positive. Therefore, we can use copper to fabricate prestressed balls with the zero or negative thermal expansion coefficient and positive temperature derivative of stiffness, which can be used for design and fabrication of particulate composites.[37]

Note that in the above analysis, the size effect of the balls filled in the shell is not rigorously studied. Instead, the effective elastic properties of the lattice is directly used in the analysis. In actual experiments, given the confining spherical shell, with the size of balls increases, the packing efficiency varies, and periodicity of microstructure and force transfer will be weaker. Therefore, the present singum prediction may exhibit errors due to the size effect.[38]

III. SINGUM MODELING OF ATOMIC LATTICES OF CUBIC CRYSTALS

Although atomic crystals exhibit different physics from granular lattices for the particle interactions and motions, if atoms are simulated by small balls with an appropriately constructed interatomic potential function, the singum model can predict the thermoelastic behaviors of the crystal lattices. When the number of balls is large enough and the lattice orientation is not uniform due to defects or non-uniformity of ball size/shape, the response tends to isotropic elasticity with static interaction.[39] As this section extends the singum model from granular lattices to crystal lattices, the two main aspects are considered: (1) the potential function of interatomic bonds for the crystal lattice shall be different from the Hertz's contact potential of Eq. (1) for granular lattices; (2) the interatomic force can be derived from the EOS and approximated by experimental data.

A. Singum potential based on the EOS of crystals with the short-range atomic interaction

Similarly to the granular lattices, when short-range atomic interactions are considered, the effective elastic tensor can be written in Eq. (12) for the three cubic lattices. Equation (14) provides the EOS of granular lattices with the Hertz's potential function in Eq. (15). Therefore, the potential function and the EOS can be correlated through the singum model. Although many interatomic potential functions in the literature[12,40] can be used to predict the elastic behavior of crystals with the short-range atomic interaction, if the EOS of the crystal is accurately characterized, we can also use the singum model to derive the potential function as well, which is called the singum potential.

The equation of state (EOS) of solids describes the volume or density change of solids with a hydrostatic pressure over a large

range[4,5] at a certain temperature. Given a hydrostatic stress $\sigma^m\delta_{ij}$, from the volumetric strain, we can calculate the bulk modulus as

$$k(\lambda) = \frac{c_{11}+2c_{12}}{3} = \frac{N(\lambda V_{\lambda\lambda} - 2V_\lambda)}{18v_s^0}, \tag{22}$$

where v_s^0 is the initial singum volume and N is the number of the closest neighbors for each cubic lattice as tabulated in Table I. Inversely, $V(\lambda)$ can be written in terms of $k(\lambda)$ by solving the above ordinary differential equation (ODE) as

$$V(\lambda) = \frac{18v_s^0}{N}\int_1^\lambda \lambda^2\left[\int_1^\lambda \lambda^{-3}k(\lambda)d\lambda + C\right]d\lambda + V(1), \tag{23}$$

where $V(1)$ is the interatomic potential at $\lambda = 1$, which can be disregarded for elastic modeling because it has no effects; C is an integral constant to be determined subsequently, which is zero by $V_\lambda|_{\lambda=1} = 0$; and $k(\lambda)$ can be given by the EOS of the crystal over a range of λ, which can be characterized at high pressures. In addition, Sec. III C provides EOS modeling, which uses a couple of material parameters to describe the EOS and often provides high accuracy. Therefore, once $k(\lambda)$ is given, the singum potential can be obtained in Eq. (37) when short-range interactions are considered.

Mathematically, three elastic constants of c_{11}, c_{12}, and c_{44} for the cubic symmetry should be independent for general cubic crystals. However, the prediction of them in Eq. (12) depends on two quantities of V_λ and $\lambda V_{\lambda\lambda}$ only for each cubic symmetry. Therefore, the three elastic constants are not truly independent. Actually, when only short-range interatomic forces are considered, the prediction is exact, which can be validated by a truss system with elastic bars as the bonds.[17,22] When measured c_{11}, c_{12}, and c_{44} are not consistent with the singum prediction, a numerical approximation should be used to minimize the difference. For crystal materials, long-range atomic interactions may change the stress of singum and, therefore, create additional variation from the identities, which will be discussed and addressed subsequently.

B. Formulation of elasticity with long-range atomic interactions

Given a crystal lattice configuration with an interatomic potential, the singum model can predict the three elastic constants from Eq. (12). The model can be straightforwardly extended from the short-range interactions to long-range interactions by an ergodic process, considering the interactions of all atoms. However, the potential V is required for the numerical simulation. Following Assumption 4, this study aims to obtain the closed-form solution, so that only short-range interactions are directly considered, whereas the long-range interactions will be approximately taken into account similarly to the embedded energy.[3]

When a singum is embedded into the surrounding atoms, the interactions among all other atoms and the interactions from nonmember atoms will also produce a stress to the singum, which can be approximately isotropic. Instead of going through an ergodic process, we introduce a hydrostatic stress σ_{ij}^p proportional to the pressure $p(v_s)$ on the singum as a correction to the whole stress in Eq. (5) as follows:

$$\sigma_{ij}^p = sp(v_s)\delta_{ij}, \tag{24}$$

where s is a constant to fit the material elastic behavior, so that the change of σ_{ij}^p with external loading is determined by $p(v_s)$. Mathematically, s provides another independent parameter to fit the three independent elastic constants while the singum model with the short-range interactions exhibits two independent constants. Obviously, when $s = 0$, it recovers the short-range model. Since v_s is related to density by Eq. (2) due to the constant mass of the singum, it can be also written as a function of density in parallel to the embedded-atom method (EAM).[3] Thus, $p(v_s)$ can be given by the EOS of the crystal, which will be discussed subsequently,

Given a displacement variation $\delta u_j(\mathbf{x}) = \delta d_{ij}x_i$, one can write the volume variation $\delta v_s = \delta d_{kk}v_s$ and, thus, obtain

$$\delta\sigma_{ij}^p = s\frac{dp}{dv_s}\delta v_s\delta_{ij} = s\frac{dp}{dv_s}v_s\delta d_{kk}\delta_{ij} = -sk(\lambda)\lambda^2\delta\varepsilon_{kk}\delta_{ij}, \tag{25}$$

where the bulk modulus $k(\lambda)$ is expressed as

$$k(\lambda) = \frac{c_{11}+2c_{12}}{3}, \tag{26}$$

with the aid of Eq. (9). Therefore, the modified stiffness can be written as

$$\overline{C}_{ijkl} = C_{ijkl} - sk(\lambda)\lambda^2\delta_{ij}\delta_{kl}, \tag{27}$$

where the overbar $(-)$ shows the relevant quantity considered by the long-range atomic interactions to differentiate from C_{ijkl} in Eqs. (11) or (12) for FCC, BCC, and SC. Therefore, when $V(\lambda)$, s, and the EOS are given, the stiffness tensor can be explicitly obtained by the above equation.

C. The equation of state of crystals

There are many analytic and semi-empirical forms of EOS in the literature.[5,41] The Vinet EOS[42] and Murnaghan–Birch (MB) EOS[24] have been widely used for the simplicity and accuracy. Although other forms of EOS can also be used for the singum model, this paper focuses on these two and we found that the MB EOS may provide more flexibility to fit the experimental results. Because $v_s = \lambda^3 v_s^0$, one can rewrite $p(v_s)$ in form of $p(\lambda)$ equivalently. The Vinet EOS is provided as follows:

$$p(\lambda) = 3k_0(1-\lambda)\lambda^{-2}e^{\eta(1-\lambda)}, \tag{28}$$

where k_0 being the bulk modulus at $\lambda = 1$ and $\eta = \frac{3}{2}(k_0' - 1)$ in which $k_0' = \frac{dk}{dp}|_{\lambda=1}$. For general solids,[43] $k_0' > \frac{5}{3}$ and $\eta > 1$, we can obtain

$$k(\lambda) = -v\frac{dp}{dv} = -v\frac{dp}{d\lambda}\frac{d\lambda}{dv} = k_0\frac{2+(\eta-1)\lambda-\eta\lambda^2}{\lambda^2}e^{\eta(1-\lambda)}, \tag{29}$$

where $v_s = \lambda^3 v_s^0$ is the deformed volume of the singum under the hydrostatic pressure. Note that the EOS is typically calibrated by the compressive stress to a fairly high pressure while the tensile stress or negative pressure is not considered. The EOS may not be valid for extremely high pressure, and there is an applicable minimal limit[43] of v_s/v_s^0 in the range of 0.45 to 0.8, which is corresponding to $\lambda_{\min}$ in the range of 0.77 to 0.93. For $\lambda_{\min} \le \lambda \le 1$, the coefficient of correlation with the experimental data of 29 kinds of metals can mostly reach 99% or higher. On the other hand, there is an extreme value for expansion,

$$\lambda_{\max} = \frac{\eta - 1 + \sqrt{(\eta-1)^2 + 8\eta}}{2\eta}, \tag{30}$$

where $k|_{\lambda=\lambda_{\max}} = 0$, which is not physical for solids anymore and could be related to the phase change of materials.

Therefore, the Vinet EOS of $k(\lambda)$ could only be applicable over the domain $\lambda_{\min} < \lambda < \lambda_{\max}$. From Eq. (30), $\lambda_{\max}$ depends on η in the range of $(1, \sqrt{2})$. Unlike gas with $0 < \lambda < \infty$, the singum potential will be defined over $\lambda_{\min} < \lambda < \lambda_{\max}$. Although the Vinet EOS is used for general solids of $\lambda \in (0.8, 1.2)$, in most engineering applications the neighborhood range is indeed limited within $\lambda = \lambda^u \pm 0.005$, where $\lambda^u = l_p^u/l_p^0$ is the bond length ratio at the undeformed state.

The MB EOS was derived by thermodynamics in a series form with tailorable accuracy to fit the experimental results, and it can be written by truncating up to the fourth-order term as follows:[23,24]

$$p = \frac{3k_0}{2}\left(\lambda^{-7} - \lambda^{-5}\right)\left[1 + \frac{3}{4}\eta_1\left(\lambda^{-2}-1\right) + \frac{3}{8}\eta_2\left(\lambda^{-2}-1\right)^2\right] \tag{31}$$

and

$$k(\lambda) = \frac{k_0}{2}\left\{\left(7\lambda^{-7} - 5\lambda^{-5}\right)\left[1 + \frac{3}{4}\eta_1\left(\lambda^{-2}-1\right) + \frac{3}{8}\eta_2\left(\lambda^{-2}-1\right)^2\right] + \frac{3}{2}\left(\lambda^{-9} - \lambda^{-7}\right)\left[\eta_1 + \eta_2\left(\lambda^{-2}-1\right)\right]\right\} \tag{32}$$

where $\eta_1 = k_0' - 4$ and $\eta_2 = k_0 k_0'' + k_0'^2 - 7k_0' + \frac{143}{9}$. Compared with the Vinet EOS, the MB EOS exhibits more constants to fit the experiments with the extension to higher order terms of strain.[44] It provides tailorable accuracy by keeping more or less terms. For example, by setting $k_0' = 4$, $k_0'' = -\frac{35}{9k_0}$, the MB EOS can be reduced to a very concise form with $\eta_1 = \eta_2 = 0$. In most applications, the third-order MB EOS is used with $\eta_2 = 0$, in which Eq. (32) can be rewritten as

$$k(\lambda) = \frac{k_0}{2}\left[\left(\frac{k_0'}{4} - 1\right)\frac{27}{\lambda^9} - \left(\frac{3k_0'}{2} - 7\right)\frac{7}{\lambda^7} + \left(\frac{3k_0'}{4} - 4\right)\frac{5}{\lambda^5}\right]. \tag{33}$$

Because the MB EOS is written in a polynomial form, it can accommodate the modeling of materials with a larger range of bond length change for ductile materials under negative pressures, although it has not been experimentally studied yet.

Figure 5 shows comparison of bulk modulus change with λ predicted by the Vinet EOS, the third-order MB EOS, the Couchman–Reynolds EOS,[43] and the Fermi energy[19] under the condition of $k_0' = 3.0$. Because the three EOS are based on k_0 and k_0', they provide almost the same predictions at the neighborhood of $\lambda = 1$. The Vinet EOS and MB EOS provide very close predictions when $0.9 < \lambda < 1.4$. When $\lambda \approx 1.2$, they predict $k = 0$, which means the loss of the stability of the crystal structure and no physical meaning for $\lambda > 1.2$ anymore. However, the Fermi energy is independent of k_0'[8,19] and is not subject to the limits of $\lambda_{\min}$ and $\lambda_{\max}$,[19] so that it can mathematically provide an interatomic potential over the full range of $(0, +\infty)$, although the accuracy is open to question as it shows a large discrepancy from the other three cases. Note that the range of $\lambda > 1$ is not validated by any experiments yet.

Indeed, the bond length in a crystal cannot be compared with the liquid or gas phase with a large range of λ, the coverage of the singum interatomic potential shall be consistent with the EOS, because it predicts the relation of stress–strain variation at the corresponding bond length or pressure. Therefore, this paper will mainly focus on the range of $\lambda \in (0.75, 1.25)$ in comparison to the two forms of EOS. In addition, although most existing EOS functions in the literature use the zero degree of temperature as the reference coordinate,[45] this paper does not consider the kinetic energy or dynamic effect of the atoms but use the zero-force bond length l_p^0 as the reference coordinate. Due to the surface energy, the undeformed state without external loading will be different from the reference state. Therefore, the parameters in the EOS will be different from those in the literature using the undeformed state as the reference coordinate.

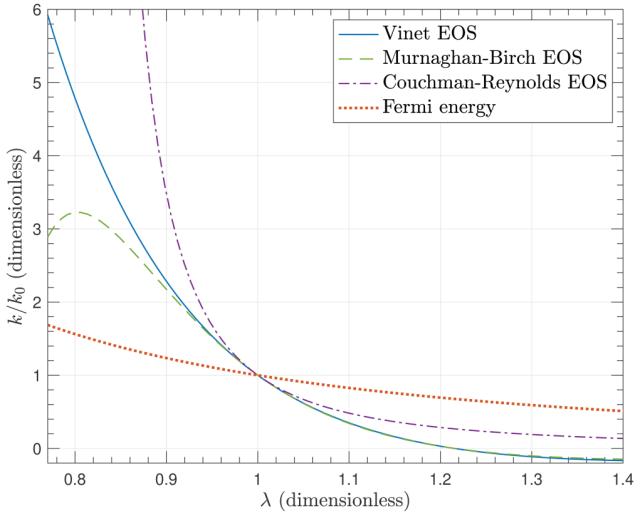

FIG. 5. The comparison of bulk modulus changing with λ predicted by the Vinet EOS, the Murnaghan–Birch EOS, the Couchman–Reynolds EOS, and the Fermi energy when $k_0' = 3$.

IV. THE INTERATOMIC POTENTIAL BASED ON THE EOS AND ELASTIC CONSTANTS

Although it is challenging to characterize the interatomic potential directly, because the singum model provides an explicit formulation to correlate the potential with the elastic behavior of the crystal, one can use the elastic behavior, which can be physically characterized for the EOS of $p(\lambda)$ and three independent elastic constants c_{11}, c_{12}, and c_{44} at the undeformed state, to inversely derive the interatomic potential. Obviously, the interatomic potential function will depend on the form of EOS. In the following, we will derive the singum potential based on the Vinet EOS and MB EOS, but the MB EOS-based potential is recommended for the flexibility and stability.

A. The singum potential based on the EOS

Substituting Eq. (11) into (27), one can obtain

$$\begin{aligned}\overline{C}_{ijkl} = &\left(c_{12} - sk(\lambda)\lambda^2\right)\delta_{ij}\delta_{kl} + (c_{11} - c_{12} - 2c_{44})\delta_{IK}\delta_{ij}\delta_{kl} \\ &+ c_{44}\left(\delta_{ik}\delta_{jl} + \delta_{jk}\delta_{il}\right),\end{aligned} \tag{34}$$

from which the three elastic constants can be rewritten in terms of the derivatives of $V(\lambda)$ for FCC, BCC, and SC, respectively, as follows:

$$\begin{aligned}\bar{c}_{11} &= \frac{\lambda V_{\lambda\lambda} + V_\lambda}{4\sqrt{2}l_p^{0^3}} - sk(\lambda)\lambda^2;\ \frac{\lambda V_{\lambda\lambda} + 2V_\lambda}{8\sqrt{3}l_p^{0^3}} - sk(\lambda)\lambda^2;\ \frac{\lambda V_{\lambda\lambda}}{8l_p^{0^3}} - sk(\lambda)\lambda^2 \\ \bar{c}_{12} &= \frac{\lambda V_{\lambda\lambda} - 5V_\lambda}{8\sqrt{2}l_p^{0^3}} - sk(\lambda)\lambda^2;\ \frac{\lambda V_{\lambda\lambda} - 4V_\lambda}{8\sqrt{3}l_p^{0^3}} - sk(\lambda)\lambda^2;\ -\frac{V_\lambda}{8l_p^{0^3}} - sk(\lambda)\lambda^2 \\ \bar{c}_{44} &= \frac{\lambda V_{\lambda\lambda} + 3V_\lambda}{8\sqrt{2}l_p^{0^3}};\ \frac{\lambda V_{\lambda\lambda} + 2V_\lambda}{8\sqrt{3}l_p^{0^3}};\ \frac{V_\lambda}{8l_p^{0^3}}.\end{aligned} \tag{35}$$

Because $k(\lambda)$ is given by the EOS if any of the three elastic constants can be given as a function of λ, one can derive $V(\lambda)$ from the corresponding ordinary differential equation (ODE) in Eq. (35). However, three constants in Eq. (35) shall be measured in experiments by an infinitesimal test load considering the nonlinear elastic nature,[44] and the change of a single elastic constant with λ may not be measured by a simple test. For instance, the shear modulus $c_{44}(\lambda)$ can be measured by a simple shear test. However, a large shear in the lattice can distort the relative position of atoms, which may lead to lattice transformation and singum annihilation. Therefore, we cannot simply use Eq. (35) to inversely derive V.

However, a hydrostatic load causes the uniform change of the lattice structure and the singum remains stable. Therefore, we can use the bulk modulus to construct the new interatomic potential. Given a hydrostatic stress $\sigma^m\delta_{ij}$, from the volumetric strain, we can calculate the bulk modulus as

$$k(\lambda) = \frac{\bar{c}_{11} + 2\bar{c}_{12}}{3} = \frac{N(\lambda V_{\lambda\lambda} - 2V_\lambda)}{18v_s^0} - sk(\lambda)\lambda^2. \tag{36}$$

If $k(\lambda)$ is given by the EOS, the singum interatomic potential can be inversely derived from Eq. (36),

$$V(\lambda) = \frac{18v_s^0}{N}\int_1^\lambda \lambda^2\left[\int_1^\lambda \lambda^{-3}k(\lambda)\left(1 + s\lambda^2\right)d\lambda + C\right]d\lambda + V(1), \tag{37}$$

where $V(1)$ is the interatomic potential at $\lambda = 1$, which will be disregarded in the subsequent part of this paper as it does not change the elasticity that depends on the derivatives of $V(\lambda)$; C is an integral constant that can be determined by $C = \frac{N}{18v_s^0}V_\lambda|_{\lambda=1} = 0$. Therefore, given EOS $k(\lambda)$, the closed-form of the singum potential can be obtained.

For the convenience of derivation, we can write the derivatives of $V(\lambda)$ as

$$\begin{aligned}V_\lambda &= \frac{18v_s^0\lambda^2}{N}\int_1^\lambda \lambda^{-3}k(\lambda)\left(1 + s\lambda^2\right)d\lambda \\ V_{\lambda\lambda} &= \frac{18v_s^0}{N}\left[2\lambda\int_1^\lambda \lambda^{-3}k(\lambda)\left(1 + s\lambda^2\right)d\lambda + \lambda^{-1}k(\lambda)\left(1 + s\lambda^2\right)\right],\end{aligned} \tag{38}$$

where Eq. (36) can be confirmed by substituting Eq. (38) into it.

B. Correlation between the elastic constants, EOS, and singum potential

As the interatomic potential and its derivatives are given by Eqs. (37) and (38) in terms of EOS $k(\lambda)$, the elastic constants can be explicitly derived by substituting Eq. (38) into Eq. (35): For FCC,

$$\begin{aligned}\bar{c}_{11}^{FCC}(\lambda) &= \tfrac{3}{2}\left[k(\lambda)(1 + s\lambda^2) + 3\lambda^2\int_1^\lambda \lambda^{-3}k(\lambda)\left(1 + s\lambda^2\right)d\lambda\right] - sk(\lambda)\lambda^2 \\ \bar{c}_{12}^{FCC}(\lambda) &= \tfrac{3}{4}\left[k(\lambda)(1 + s\lambda^2) - 3\lambda^2\int_1^\lambda \lambda^{-3}k(\lambda)\left(1 + s\lambda^2\right)d\lambda\right] - sk(\lambda)\lambda^2 \\ \bar{c}_{44}^{FCC}(\lambda) &= \tfrac{3}{4}\left[k(\lambda)(1 + s\lambda^2) + 5\lambda^2\int_1^\lambda \lambda^{-3}k(\lambda)\left(1 + s\lambda^2\right)d\lambda\right].\end{aligned} \tag{39}$$

For BCC,

$$\begin{aligned}\bar{c}_{11}^{BCC}(\lambda) &= k(\lambda)\left(1 + s\lambda^2\right) + 4\lambda^2\int_1^\lambda \lambda^{-3}k(\lambda)\left(1 + s\lambda^2\right)d\lambda - sk(\lambda)\lambda^2 \\ \bar{c}_{12}^{BCC}(\lambda) &= k(\lambda)\left(1 + s\lambda^2\right) - 2\lambda^2\int_1^\lambda \lambda^{-3}k(\lambda)\left(1 + s\lambda^2\right)d\lambda - sk(\lambda)\lambda^2 \\ \bar{c}_{44}^{BCC}(\lambda) &= k(\lambda)\left(1 + s\lambda^2\right) + 4\lambda^2\int_1^\lambda \lambda^{-3}k(\lambda)\left(1 + s\lambda^2\right)d\lambda.\end{aligned} \tag{40}$$

For SC,

$$\begin{aligned}\bar{c}_{11}^{SC}(\lambda) &= 3k(\lambda)\left(1+s\lambda^2\right)+6\lambda^2\int_1^\lambda \lambda^{-3}k(\lambda)\left(1+s\lambda^2\right)d\lambda - sk(\lambda)\lambda^2\\ \bar{c}_{12}^{SC}(\lambda) &= -3\lambda^2\int_1^\lambda \lambda^{-3}k(\lambda)\left(1+s\lambda^2\right)d\lambda - sk(\lambda)\lambda^2\\ \bar{c}_{44}^{SC}(\lambda) &= 3\lambda^2\int_1^\lambda \lambda^{-3}k(\lambda)\left(1+s\lambda^2\right)d\lambda.\end{aligned} \tag{41}$$

Therefore, given the reference bond length $2l_p^0$ at the zero force state ($\lambda = 1$) and the EOS of $k(\lambda)$, one can calculate the elastic constants changing with the bond length λ or pressure. When the Vinet EOS in Eq. (29) is used, the potential is

$$V(\lambda) = \frac{18v_s^0k_0}{N}\int_1^\lambda \lambda^2\left[\int_1^\lambda \frac{2+(\eta-1)\lambda-\eta\lambda^2}{\lambda^5}\left(1+s\lambda^2\right)e^{\eta(1-\lambda)}d\lambda\right]d\lambda. \tag{42}$$

The integral form singum potential can be explicitly written in terms of the exponential integral function,[19,46] which is similar to but more complex than the Morse potential.[40] When the third-order MB EOS in Eq. (33) is used, one can write

$$V(\lambda) = \frac{9v_s^0k_0}{N}\int_1^\lambda \lambda^2\int_1^\lambda\left[\left(\frac{k_0'}{4}-1\right)\frac{27}{\lambda^{12}}-\left(\frac{3k_0'}{2}-7\right)\frac{7}{\lambda^{10}}+\left(\frac{3k_0'}{4}-4\right)\frac{5}{\lambda^8}\right] \times\left(1+s\lambda^2\right)d\lambda d\lambda, \tag{43}$$

which can be explicitly written in terms of a polynomial of λ, which is similar to but more complex than the LJ potential.[47,48] Given k_0 and k_0', once the Vinet or MB EOS is chosen to determine $p(\lambda)$ or $k(\lambda)$, the potential function of $V(\lambda)$ is obtained with unknown s, while both $V(\lambda)$ and the EOS of $k(\lambda)$ refer to the equilibrium bond length $2l_p^0$, which is another unknown.

In practical applications, given a crystal with the lattice type and atom mass, one can measure the three elastic constants $\bar{c}_{11}$, $\bar{c}_{12}$, and $\bar{c}_{44}$ at the undeformed state with the density or l_p^u known as well. The EOS behavior can be measured as a function of $p(v_s)$, which can be transferred into $k(l_p)$ with l_p varying in a certain range. Using the FCC lattice as an example, the following steps can be used to determine l_p^0, s, k_0, and k_0', which can define $k(\lambda)$, $V(\lambda)$, and $\mathbf{C}(\lambda)$:

(1) Although $\lambda^u = l_p^u/l_p^0$ is not determined with l_p^0 unknown yet, from three equations in Eq. (39), we obtain

$$s = \frac{3}{(\lambda^u)^2}\frac{\bar{c}_{12}^u - 2\bar{c}_{11}^u + 3\bar{c}_{44}^u}{\bar{c}_{11}^u + 2\bar{c}_{12}^u}, \quad k(\lambda^u) = \frac{\bar{c}_{11}^u + 2\bar{c}_{12}^u}{3}, \tag{44}$$

where λ^u must satisfy

$$(\lambda^u)^2\int_1^{\lambda^u}\lambda^{-3}k(\lambda)\left(1+s\lambda^2\right)d\lambda = \frac{\bar{c}_{11}^u - \bar{c}_{12}^u - \bar{c}_{44}^u}{3}. \tag{45}$$

(2) When $k(\lambda)$ is selected for the EOS, k_0 can be written in terms of $k(\lambda^u)$ and k_0'. For example, if the MB EOS is used with Eq. (32), k_0 can be written as

$$k_0 = \frac{4k(\lambda^u)}{\left[\frac{7}{(\lambda^u)^7}-\frac{5}{(\lambda^u)^5}\right]\left[2+\frac{3\eta_1}{2}\left(\frac{1}{(\lambda^u)^2}-1\right)+\frac{3\eta_2}{4}\left(\frac{1}{(\lambda^u)^2}-1\right)^2\right]+\left[\frac{3}{(\lambda^u)^9}-\frac{3}{(\lambda^u)^7}\right]\left[\frac{\eta_2}{(\lambda^u)^2}+\eta_1-\eta_2\right]}, \tag{46}$$

while k_0 of the Vinet EOS can be written as follows:

$$k_0 = \frac{k(\lambda^u)e^{-\frac{3}{2}(k_0'-1)(1-\lambda^u)}(\lambda^u)^2}{2+\left[\frac{3}{2}(k_0'-1)-1\right]\lambda^u-\frac{3}{2}(k_0'-1)(\lambda^u)^2}. \tag{47}$$

(3) As k_0' generally in the range of (2,10),[4] a numerical iteration method is used to search k_0' and l_p^0 to minimize the standard deviation of $p(v_s)$ from the experimental results as follows:
   (a) Assuming $l_p^0 = l_p^u$, use either the Vinet or MB EOS $p(\lambda)$ to fit the experimental data, and obtain, thus, k_0' as well as the standard deviation (σ^0) between the fitted function and the experimental results.
   (b) Use k_0' and k_0 in Eq. (46) or (47) to construct EOS $k(\lambda)$ and substitute it into Eq. (45). Therefore, λ^u is the only unknown in Eq. (45) and can be determined. Although multiple solutions may exist, the one close to 1 shall be the solution.
   (c) Use λ^u to update l_p^0 and repeat steps (a) and (b) to update the EOS $p(\lambda)$ and calculate the standard deviation (σ^i) from the experimental results and λ^u until the convergence of λ^u and σ^i.

4. Ideally, given the cubic symmetric elastic constants of an FCC lattice at the undeform state, one can determine the zero-force bond length l_p^0 by λ^u and then the EOS $k(\lambda)$ and the interatomic potential $V(\lambda)$.

Note that if higher order EOS is used, such as Eq. (32) with the derivative k_0'' of the bulk modulus, the above procedure can be straightforwardly extended with better curve fitting accuracy of the experimental data. Otherwise, it is possible to obtain nonphysical results such as $k_0 < 0$ through the mathematical calculation.

As the same procedure can be also applied for other lattices, Eqs. (44) and (45) shall be updated as follows:

For BCC,

$$s = \frac{3}{(\lambda^u)^2}\frac{\bar{c}^u_{44} - \bar{c}^u_{11}}{\bar{c}^u_{11} + 2\bar{c}^u_{12}}, \quad k(\lambda^u) = \frac{\bar{c}^u_{11} + 2\bar{c}^u_{12}}{3}, \tag{48}$$

where λ^u must satisfy

$$(\lambda^u)^2 \int_1^{\lambda^u} \lambda^{-3} k(\lambda)\left(1 + s\lambda^2\right) d\lambda = \frac{\bar{c}^u_{11} - \bar{c}^u_{12}}{6}. \tag{49}$$

For SC,

$$s = -\frac{3}{(\lambda^u)^2}\frac{\bar{c}^u_{12} + \bar{c}^u_{44}}{\bar{c}^u_{11} + 2\bar{c}^u_{12}}, \quad k(\lambda^u) = \frac{\bar{c}^u_{11} + 2\bar{c}^u_{12}}{3}, \tag{50}$$

where λ^u must satisfy

$$(\lambda^u)^2 \int_1^{\lambda^u} \lambda^{-3} k(\lambda)\left(1 + s\lambda^2\right) d\lambda = \frac{\bar{c}^u_{44}}{3}. \tag{51}$$

Mathematically, we can determine λ^u, s, k_0, k_0', and k_0'' (for MB EOS) by the experimental results of the elastic constants and EOS, which may exhibit multiple acceptable solutions. The selection of the appropriate solution shall follow the physical meaning. As demonstrated in Sec. IV, the applicable ranges of those parameters are as follows: $\lambda^u \in (0.75, 1.25)$, $s > -1/\lambda^u$, $k_0 > 0$, and $k_0' > 0$.

C. Orientational average of elasticity for isotropic polycrystals

In materials engineering, metals, such as steel, aluminum, or copper, are commonly considered to be isotropic with two independent elastic constants, such as the Young's modulus and Poisson's ratio, even though they exhibit cubic lattices at the atomic scale. For example, steel exhibits the BCC lattice, while aluminum or copper is the FCC lattice. In the bulk materials, the crystals form anisotropic grains, which are not aligned in the same orientation during the manufacture process with impurities, defects, or fillers. Therefore, the overall material behavior is indeed isotropic. Considering the randomness of the grain's orientation, an orientational average[26,49] is applied to Eq. (35), the anisotropic terms will be averaged out, so that one can obtain an isotropic elasticity with two independent parameters,[19]

$$k = \frac{\bar{c}_{11} + 2\bar{c}_{12}}{3} \quad \text{and} \quad \mu = \frac{\bar{c}_{11} - \bar{c}_{12} + 3\bar{c}_{44}}{5}, \tag{52}$$

from which all isotropic elastic constants, such as Young's modulus and Poisson's ratio, can be calculated,[50] respectively, as follows:

$$E = \frac{9k\mu}{3k + \mu} \quad \text{and} \quad \nu = \frac{3k - 2\mu}{2(3k + \mu)}. \tag{53}$$

Here, μ can be further written in terms of the derivatives of the interatomic potential as

$$\mu = \frac{N(\lambda V_{\lambda\lambda} + 4V_\lambda)}{30v_s^0} = \frac{3}{5}\left[k(\lambda)\left(1 + s\lambda^2\right) + 6\lambda^2 \int_1^{\lambda} \lambda^{-3} k(\lambda)\left(1 + s\lambda^2\right) d\lambda\right], \tag{54}$$

which is applicable to all three cubic crystals. In polycrystals, the elastic constants are affected by material processes such as heat treatment and work hardening, which may change the effective bond length and crystal lattice configuration. In addition, the grain size also significantly affects the mechanical properties of metals. The above formulation may not catch those effects directly. Instead, we assume the long-range interactions or s shall be different from the single crystal, so that we can fit the experimental data with s to provide an empirical way to correlate the relationship of the two isotropic elastic constants, EOS, and the interatomic potential as well.

Note that each grain in polycrystal may exhibit a different prestress state due to the different size and orientations and the overall undeformed state is an average of all the states, so the experimental data can only provide empirical prediction instead of the fundamental material constants. Because the atom equilibrium bond length $2l_p^0$ shall be the same for single crystal or polycrystal, $2l_p^0$ can be used as a given material constant. Given two elastic constants k and μ and the EOS experimental data at the undeformed state λ^u as well as the EOS data of $p(\lambda^i)$ with i indicating the number of testing data, one can conduct curve fitting of EOS $k(\lambda)$ and back calculate s from Eq. (54) by $\mu(\lambda^u)$. With s calculated, $V(\lambda)$ can be obtained from Eq. (37) or by solving the ODE of Eq. (54).

For a new polycrystal with EOS $p(\lambda^i)$ but $2l_p^0$ unknown, the above procedure cannot be implemented, as l_p^0 and s cannot be determined by a single elastic constant $\mu(\lambda^u)$. When the long-range atomic interaction is disregarded due to the grain boundary effect, one could assume $s = 0$ and then the similar procedure to determine l_p^0 and $V(\lambda)$ in the last subsection for single crystals can be applied to polycrystals as well, but Eq. (45), (49), or (51) shall be updated as follows:

$$(\lambda^u)^2 \int_1^{\lambda^u} \lambda^{-3} k(\lambda) d\lambda = \frac{1}{6}\left[\frac{5\mu(\lambda^u)}{3} - k(\lambda^u)\right], \tag{55}$$

which leads to the explicit EOS with k_0 written in terms of $k(\lambda^u)$ and λ^u.

Note that because polycrystal's elastic behavior is an average of the single crystal's elastic behavior at different stress states, it is empirical for the specific fabrication process and material batch and shall not be generalized to all types of polycrystals, which indeed exhibit different elastic behavior in a relatively large spectrum compared with the corresponding single crystal.

Interestingly, although the single crystals for the three cubic lattices exhibit different trends of elasticity in Eqs. (39)–(41), their polycrystals share the same form of isotropic constants related to the interatomic potential and EOS as Eqs. (36) and (54). Note that the orientational average of elasticity in the singum model is not limited to the cubic crystals.[19] Mathematically, given any number

of the closest neighboring atoms, we can establish the relationship of the generalized singum potential and two isotropic elastic constants and, thus, derive the singum potential function from the elastic constants.

V. RESULTS AND DISCUSSION

Although this singum model only directly considers the short-range interatomic forces with an embedded energy for the long-range atomic interactions because the short-range interaction is indeed dominate in solids, the model can capture the physics and mechanics of solids with good fidelity. Particularly, because the singum interatomic potential is derived and calibrated by the elastic behavior, the accuracy of the model may reach the engineering standard. Obviously, the volume-surface ratio of a continuum particle will play a role on its effective elasticity due to the boundary effect when it is small. However, the lattice structure and effective elasticity of crystals are fairly stable with size reduction to the nanoscale.[51] It indicates that the long-range atom interactions play a minor role in the solid states, which is much less important than in the liquid or gas states. The proposed singum model approximates the long-range interactions by a pressure to provide a closed form solution. On the other hand, the Vinet EOS is only applicable to a small range of λ as well, which produces difficulties to accurately consider the long-range atomic interactions by an ergodic process. This section first demonstrates the singum model for coppers with the two forms of EOS[4,24,43] and use them to predict the anisotropic elastic constants in comparison to the experimental results. The temperature and pressure derivatives of the elasticity are then calculated from the singum model, which can predict thermoelastic constants of metals at different temperature. Particularly, it is important for geothermal and fire-safety applications[16] when engineering metals are used for load bearing under high pressures and temperatures. In this section, we use copper as an example for demonstration, which can be straightforwardly generalized to other engineering metals in the supplementary material.

A. Demonstration of the singum potential for single crystalline copper

Given the atomic lattice and elastic constants of a metal measured without external stress at a certain temperature, we can use the lattice and elastic constants to construct the singum potential function $V(\lambda)$. Using the singum potential, we can predict the elastic behavior changing with the bond length ratio λ, which depends on pressure and temperature for different applications. Fortunately, most metals exhibit well established atomic lattice and density, and their EOS parameters were investigated in the literature as well. Therefore, the singum potential for common metals can be established and can predict the thermoelastic behavior which may not be available in the literature yet.

Ledbetter and Naimon[52] conducted a comprehensive literature review of the experiments of copper by the time, which will be used for singum model construction and validation. The following material constants measured at the room temperature (300 K) will be used: Density $\rho^{Cu} = 8.937 \times 10^3\,\mathrm{kg/m^3}$; the FCC lattice with $N = 12$ members and atom weight $M_a = 10.552 \times 10^{-26}$ kg, $c_{11} = 169.1$ GPa, $c_{12} = 122.2$ GPa, $c_{44} = 75.42$ GPa; for the polycrystal, Young's modulus $E^{Cu} = 124.7$ GPa, Poisson's ratio $\nu^{Cu} = 0.35$, and thermal expansion coefficient $\alpha^{Cu} = 16.5 \times 10^{-6}\,\mathrm{K^{-1}}$.

Using the above data, we can calculate the Lame constants from the isotropic elastic constant relationship,[50] as $\lambda^{Cu} = 107.80$ GPa, $\mu^{Cu} = 46.2$ GPa, the bulk modulus $k^{Cu} = 138.6$ GPa, the bond length $2l_p^u = 0.2556$ nm, and the singum volume $v_s = 1.1808 \times 10^{-29}\,\mathrm{m^3}$.[19]

In the following, we can use the three elastic constants for a single FCC crystal to determine EOS and the interatomic potential. The experimental measurements for the EOS of copper have been conducted by authors in Ref. 53. Following the four steps with the Vinet EOS in Sec. III B, we can determine $\lambda^u = 0.7532$, $k_0 = 1.089$ GPa, and $k_0{}' = 9.17$, which lead to $l_p^0 = 1.697$ Å, $v_s^0 = 27.63\,\mathrm{Å^3}$, $\eta = 12.3$, and $s = 0.1312$. Thus, the closed-form EOS and singum potential can be obtained from Eqs. (28), (29), and (42) as

$$\begin{aligned} p^{Vinet}(\lambda) &= 3 \times 1.089 \frac{(1-\lambda)}{\lambda^2} e^{12.3(1-\lambda)} + 29.16, \\ k^{Vinet}(\lambda) &= 1.089 \left[\frac{2+(12.3-1)\lambda - 12.3\lambda^2}{\lambda^2}\right] e^{12.3(1-\lambda)}, \\ V^{Vinet}(\lambda) &= 3.80 \times 10^{-28} \int_1^{\lambda} \lambda^2 \\ &\quad \times \left[\int_1^{\lambda} \frac{2+11.3\lambda - 12.3\lambda^2}{\lambda^5}\left(1+0.1312\lambda^2\right) e^{12.3(1-\lambda)} d\lambda\right] d\lambda. \end{aligned} \tag{56}$$

Using $\lambda = \left(v_s/v_s^0\right)^{1/3}$, the $p-v$ graph can be plotted as shown in Fig. 6, and the above formulation can reproduce the measured

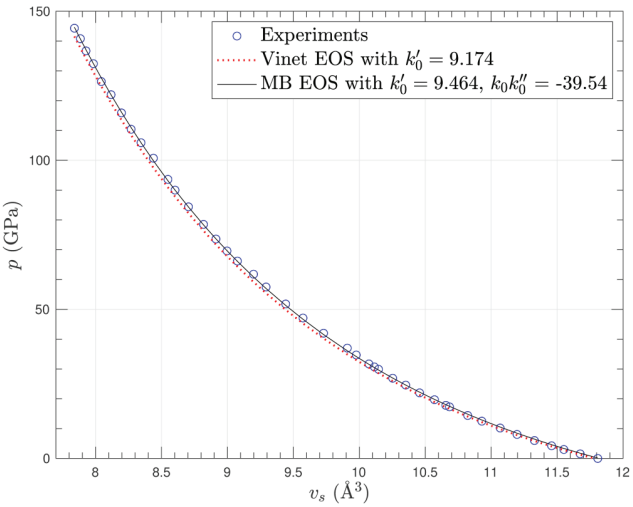

FIG. 6. The pressure changing with the singum volume ($p - v$) by the Vinet EOS when $\lambda^u = 0.7532$, $k_0 = 1.089$ GPa, and $k_0' = 9.17$ (dot line) and the MB EOS when $\lambda^u = 0.7765$, $k_0 = 2.521$ GPa, $k_0' = 9.464$, and $k_0k_0'' = -39.54$ (solid line) in comparison to the experiments of single crystalline copper (circle symbols).[53]

elastic constants exactly by Eq. (39), while the EOS equation cannot fit very well with the experimental data. Note that Dewaele *et al.*[53] provided $k_0 = 133$ GPa and $k_0' = 5.30$, which fit the experimental data excellently, but they used $l_p^0 = l_p^u$, whereas this paper differentiates them which makes $\lambda^u = 0.7532$ at the undeformed state instead of $\lambda^u = 1$. Because the Vinet EOS imposed a small range of λ, once the λ^u approaches the limit, the function may not accurately fit the experimental data. However, the MB EOS, which was derived by thermodynamics,[23,24] is more versatile to deal with a larger range of λ^u by changing the pressure derivatives including k_0', k_0'', and higher order terms as necessary. In Fig. 6, we show graphs of $\lambda^u = 0.7765$, $k_0 = 2.521$ GPa, $k_0' = 9.464$, $k_0 k_0'' = -39.54$, and $s = 0.1235$ with the experimental data.[53] Overall, the MB EOS exhibits better fitting to the experiments, and those parameters with the MB EOS will be used in the following discussion.

The EOS and the corresponding potential function for single crystalline copper are summarized as follows:

$$
\begin{aligned}
p^{MB}(\lambda) &= 3.782\left(\frac{1}{\lambda^7}-\frac{1}{\lambda^5}\right)\left[1+4.098\left(\frac{1}{\lambda^2}-1\right)-0.1258\left(\frac{1}{\lambda^2}-1\right)^2\right]+32.59,\\
k^{MB}(\lambda) &= 1.2605\left\{\left(\frac{7}{\lambda^7}-\frac{5}{\lambda^5}\right)\left[1+4.098\left(\frac{1}{\lambda^2}-1\right)-0.1258\left(\frac{1}{\lambda^2}-1\right)^2\right]-\frac{3}{2}\left(\frac{1}{\lambda^9}-\frac{1}{\lambda^7}\right)\left(\frac{0.3355}{\lambda^2}+5.799\right)\right\},\\
V^{MB}(\lambda) &= 4.768\times10^{-20}\int_1^\lambda \lambda^2\int_1^\lambda\left(\frac{7}{\lambda^{10}}-\frac{5}{\lambda^8}\right)\left[1+4.098\left(\frac{1}{\lambda^2}-1\right)-0.1258\left(\frac{1}{\lambda^2}-1\right)^2\right]\\
&\quad-\frac{3}{2}\left(\frac{1}{\lambda^{12}}-\frac{1}{\lambda^{10}}\right)\left(\frac{0.3355}{\lambda^2}+5.799\right)d\lambda d\lambda,
\end{aligned}
\tag{57}
$$

with $l_p^0 = 1.646$ Å and $v_s^0 = 25.22$ Å^3.

Figure 7 shows $V(\lambda)$ with its derivatives of $V_{,\lambda}$ and $V_{,\lambda\lambda}$ in the inset. For $\lambda < 1$, it increases faster in comparison to $\lambda > 1$, which represents a larger repulsive force than the attractive force with the same change of stretch level. Using the derivatives, one can predict the elastic constants changing with the bond length. Note that the undeformed bond length is fairly far from the bottom of the well with $\lambda^u = 0.7765$. It provides a long pathway for the atoms to separate from each other and leads to very good ductility of copper. Instead, single crystalline aluminum exhibits $\lambda^u > 1.1$,[19] which will be much more brittle than copper.

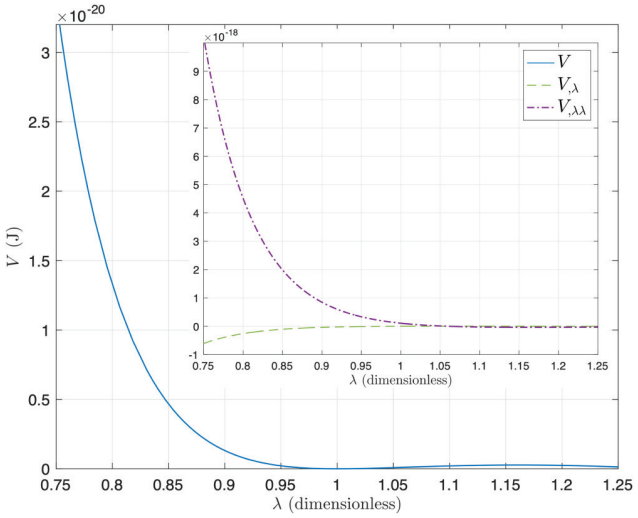

FIG. 7. The interatomic potential of copper based on the MB EOS. The inset shows its first and second derivatives.

Using the derivatives of $V_{,\lambda}(\lambda)$ and $V_{,\lambda\lambda}(\lambda)$ of Eq. (57), we can predict the elastic constants changing with λ. Figure 8 illustrates the three cubic symmetric elastic constants changing with λ. Indeed, at the undeformed state, the predictions of the three elastic constants are the same as the measurements because the potential was determined by those values. With the increase in λ, the elastic constants reduce at different rates: c_{44} changes much slower than c_{11} and c_{12}.

Notice that the effective range of λ of the singum potential obtained from the EOS is narrow, but it is sufficient to study the thermoelastic behavior of solids. To cover the full range of λ, a simple form of EOS may not exist due to the phase change of materials, which will be discussed later.

B. Application of the singum model for polycrystalline copper

In engineering design of metal structures, engineering metals are often considered as isotropic materials in forms of polycrystals.[52,54] Because polycrystalline copper's properties may vary with grain size, metal work procedure, heat treatment, etc., which may change the local lattice structure at a certain degree, a simple orientational average by Eq. (52) may provide some errors in prediction. For example, using single crystalline copper's elastic properties at the undeformed state at the room temperature, one can obtain $(c_{11}+2c_{12})/3 = 137.8$ GPa but $(c_{11}-c_{12}+3c_{44})/5 = 54.63$ GPa,

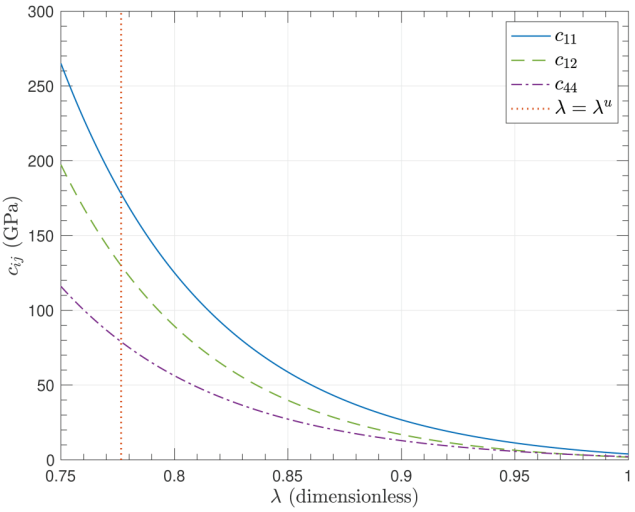

FIG. 8. The three elastic constants of single crystalline copper changing with λ, where λ^u (dot line) indicates the undeformed state.

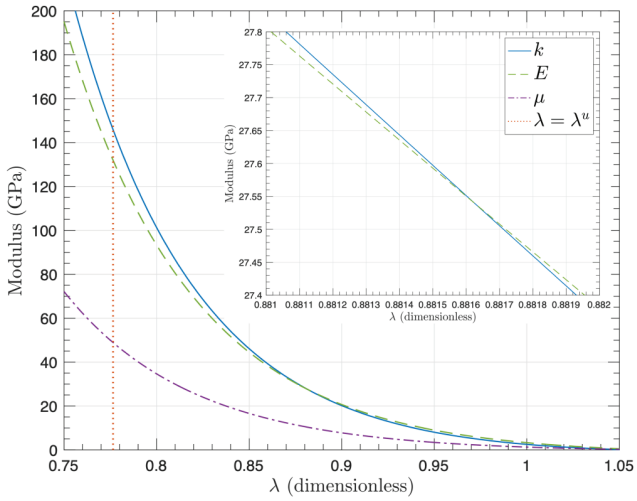

FIG. 9. The bulk modulus (solid line), Young's modulus (dashed line), and shear modulus (dashed-dotted line) of polycrystalline copper changing with λ, where λ^u (dotted line) indicates the undeformed state. The inset shows those moduli when λ is from 0.881 to 0.882.

which fits the polycrystal's bulk modulus $k = 138.6$ GPa very well, but the shear modulus of $\mu = 46.2$ GPa exhibits a difference about 8.4 GPa.

Instead of a thorough investigation of the lattice microstructure, we can still empirically use the isotropic elastic constants to back calculate s, so as to estimate the elastic constants changing with the volume or effective bond length of the polycrystal. Assume the polycrystalline copper exhibits the same density as the single crystalline copper so that they share the same λ^u on average. Using the copper interatomic potential in Eq. (57) and $\mu = 46.2$ GPa, we can back calculate $s = -0.1514$, which is different from the single crystalline copper at 0.1138. Then, we can calculate the bulk modulus and shear modulus, and then all other isotropic elastic constants[50] changing with the bond length.

Figure 9 shows the variation in the bulk modulus (k), Young's modulus (E), and shear modulus (μ) with λ. All of them decrease when the bond length increases but exhibit different rates. The bulk modulus is exactly described by the EOS and is the highest over most of the range but is overpassed by Young's modulus at $\lambda = 0.8816$. The Shear modulus stays low over the whole range of $(0.75, 1.05)$.

To describe the rate of different elastic constants, Fig. 10 illustrates Poisson's ratio changing with λ. For comparisons, it shows three cases of $s = -0.1514$, 0, and 0.1235, which are taken from the cases of polycrystal, no long-range interactions, and single crystal of copper, respectively. When $\lambda < 0.9$, the Poisson's ratio varies in a very small range. When $\lambda > 0.9$, Poisson's ratio drops rapidly for all three cases. If only short-range interactions are considered, or $s = 0$, which is shown by the solid line, we can observe that when $\lambda = 1$ or at the zero-force bond length, the Poisson's ratio $\nu = 0.25$, which is consistent with the previous work.[19,22] When the prestress is a positive pressure and $\lambda^u < 1$, $\nu > 0.25$, the crystal is more ductile. When the prestress is a negative pressure and $\lambda^u > 1$, $\nu < 0.25$, the crystal is more brittle in general. Due to the long-range interactions, this rule of $\nu = 0.25$ may not be a clear-cut, as the value also depends on s. When s increases, Poisson's ratio decreases. However, for metamaterials with exact short-range interactions, s is fixed at 0, so that $\nu = 0.25$ indeed serves a critical value to

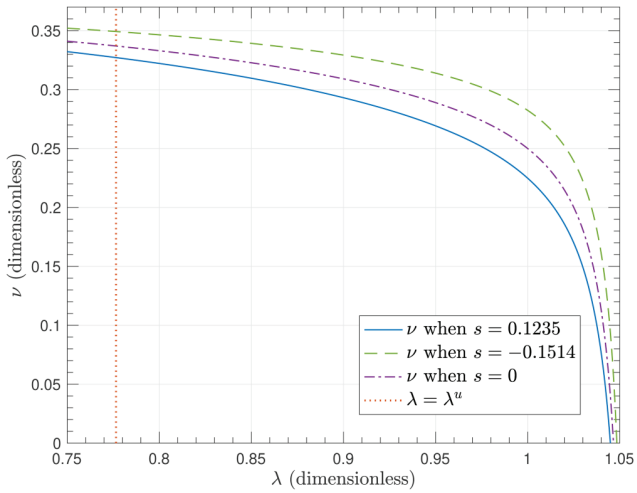

FIG. 10. The Poisson's ratio of single crystalline copper with $s = 0.1235$ (solid line), polycrystalline copper with $s = -0.1514$ (dashed line), and the short-range copper model with $s = 0$ (dashed-dotted line) changing with λ, where λ^u (dotted line) indicates the undeformed state.

determine the sign of the prestress caused by the surface tension, which can empirically determine the ductility and fracture toughness of the material if a critical bond length for fracture is given.

C. Pressure- and temperature-dependent elasticity of crystals

Figures 8 and 9 illustrate the elastic constants' change with the bond length for single crystalline and polycrystalline copper, respectively. Because λ changes with pressure, which is given through the EOS, the elasticity of solids will also change with pressure. The pressure derivatives of the elastic constants can be used to reconstruct the pressure-dependent elasticity. Actually, the EOS is often developed with the bulk modulus and its pressure derivatives in the undeformed state. It is of significance to model the pressure-dependent elasticity for engineering applications. The singum model is particularly convenient to predict the pressure-dependent elasticity and their pressure derivatives. On the other hand, thermal expansion of crystals with temperature change can also correlate with the bond length change. Although the kinetic energy of atoms may produce contributions to the elastic properties as well, it is secondary to the bond length change. This paper focuses on the effect of the averaged bond length only and the kinetic energy's contribution is disregarded.

In addition, the pressure- and temperature-dependent elasticity for single crystals can be obtained in the same fashion as polycrystals. In the following, we use polycrystals to demonstrate the calculation of the pressure- and temperature-dependent elasticity. Because the closed-form of elasticity is given, it can be easily extended to single crystalline copper and other types of cubic crystals as well.

Using the EOS $p(\lambda)$ in Eq. (57) in the effective range of λ, we can write λ as an inverse function of p, namely, $\lambda(p) = p^{inv}$. Therefore, the bulk modulus $k(\lambda)$ and shear modulus $\mu(\lambda)$ can be rewritten in terms of pressure so as to obtain the two pressure-dependent elastic constants. Using the two elastic constants, we can calculate other elastic constants at the given pressure.

Given an elastic constant, namely, $c(\lambda)$, in terms of $V_{,\lambda}$ and $V_{,\lambda\lambda}$, such as Eqs. (12), (36), and (54), one can derive the pressure derivative as follows:

$$\frac{dc(\lambda)}{dp} = \frac{dv}{dp}\frac{d\lambda}{dv}\frac{dc(\lambda)}{d\lambda} = -\frac{\lambda}{3k(\lambda)}\frac{dc(\lambda)}{d\lambda}, \tag{58}$$

where $\lambda = \left(v/v_s^0\right)^{1/3}$, $\frac{dv}{dp} = -\frac{v}{k(\lambda)}$, and $v\frac{d\lambda}{dv} = \frac{\lambda}{3}$ are used. Here, c can represent any elastic constants, such as c_{11}, c_{12}, c_{44}, k, μ, etc. Therefore, the pressure derivatives of elastic constants can be analytically obtained by the above equation.

The pressure-dependent bulk modulus can be calculated from the $p - v$ curve in Fig. 6, which was validated by the experiments under hydrostatic pressures.[55] However, it is very challenging to measure other elastic constants at high pressures. The closed-form formulation can predict its derivatives analytically. Typically, elastic constants increase with the pressure due to the stronger atomic interaction at a higher pressure.

When the temperature is higher than the Debye temperature of a solid,[45] the thermal expansion exhibits a linear range over a large temperature range, which is nearly described by the linear thermal expansion coefficient. Although the elasticity may also affect the atom vibration quantified by the temperature, the average bond length change shall play a key role on the temperature-dependent elasticity, which provides a feasibility to use the thermal expansion coefficient, namely, α, and EOS to predict the temperature-dependent elasticity of the solid and its temperature derivative.

For simplicity, when the pressure keeps at zero, the relationship of λ and temperature change T referred to the undeformed state can be written as

$$\frac{\lambda}{\lambda^u} = 1 + \alpha(T - T_0) \quad \text{or} \quad \lambda = \lambda^u[1 + \alpha(T - T_0)]. \tag{59}$$

Therefore, the temperature-dependent elastic constants of $k(T)$ and $\mu(T)$ can be analytically obtained by replacing λ with T in the above equation.

Similarly to the pressure derivatives, the temperature derivative of an elastic modulus can also be obtained by the following equation:

$$\frac{dc(\lambda)}{dT} = \frac{d\lambda}{dT}\frac{dc(\lambda)}{d\lambda} = \lambda^u\alpha\frac{dc(\lambda)}{d\lambda}. \tag{60}$$

Figure 11 shows the temperature-dependent elastic moduli using the coefficient of thermal expansion for copper[36] in comparison to the experimental results of bulk modulus (k_{exp}), Young's modulus (E_{exp}), and shear modulus (μ_{exp}),[52,56] as well as all of the three elastic constants decrease with the temperature.

Therefore, the pressure increases the elasticity by reducing λ, whereas the temperature decreases the stiffness by thermal expansion. In geothermal applications, both factors exist and the elasticity will be affected by both temperature and pressure. Again, although temperature may produce more complex effects on the elastic behavior, this paper focuses on the effect through the bond length λ. Given k_0, k_0', k_0'', and $2l_p^0$ (bond length) at the reference temperature T_0, we can write the bond length in terms of both pressure and temperature, so that the thermoelasticity of the crystal can be fully predicted. Given a temperature T and pressure p, we can calculate λ and then predict the isotropic elastic constants. Basically, the $p - \lambda$ curves at different temperatures share the same shape with a pressure shift. Therefore, the temperature and pressure derivatives can be calculated in the same fashion as the above procedure and will keep the same mathematical form, in which λ depends on both T and p instead. Notice that here we assume the thermal expansion coefficient α is a constant for different pressures as well, which can be inaccurate in actual applications, particularly under high pressures.

The present model can be applicable to other crystal lattices, and the supplementary material shows the case studies for nickel and tungsten in FCC and BCC lattices, respectively. Note that when the temperature is close to the melting point, the atomic lattice loses the stability and the material starts to change from the solid state to the liquid state. The present model may lose accuracy in those temperatures and the dynamic motion of atoms should be considered in future work. Particularly, for some metals such as

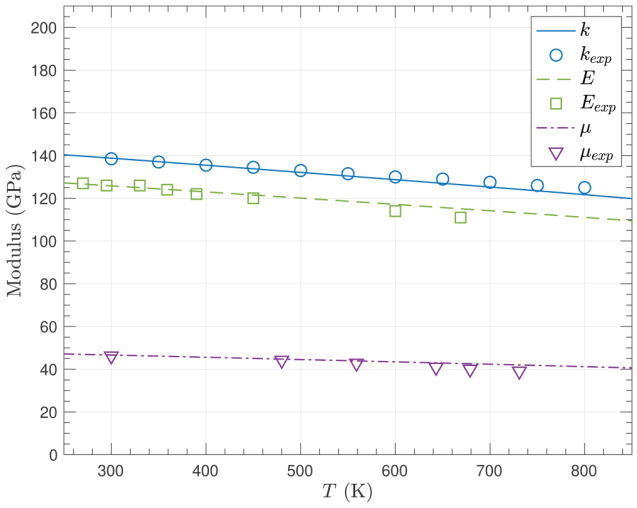

FIG. 11. The temperature-dependent isotropic elastic moduli of polycrystalline copper: bulk modulus (solid line), Young's modulus (dashed line), and shear modulus (dashed-dotted line) with the experimental results for bulk modulus (circle symbols), Young's modulus (square symbols), and shear modulus (triangle symbols).

iron, it will undergo phase transformation with the increase in pressure and temperature. In this case, a multiphase singum model may be required to reproduce the elastic modulus and melting temperature in accordance with the phase change.

D. Discussion about the EOS-based singum model

This paper uses the EOS to construct the singum potential. Because the Vinet EOS and MB EOS have established accuracy over a large range of compressibility, which is much more than the typical stress states in the engineering applications, the formulation can provide high fidelity predictions to the thermoelasticity of metal solids, which is taken into account by the change of λ. Although the singum model does not consider the actual atomic dynamics with temperature change, the results demonstrated by copper are in line with the mechanics and physics of solids. The elasticity increases with pressures but decreases with temperatures. The changing rates of different elastic moduli are different as clearly demonstrated in Fig. 9, which can be quantified by the Poisson's ratio in Fig. 10. The singum model is developed by rigorous mechanical analysis of the local forces. Although only short-range interactions are directly considered to provide a closed-form prediction of the thermoelastic properties of crystals, the long-range interactions are taken into account approximately. It analytically correlates the elastic constants, EOS, and interatomic potential. An ergodic process considering all particle interactions may improve the accuracy of the singum model in future work. The present model can disclose the mechanics and physics of cubic crystals and creates some research areas as follows:

(1) The singum model is general. Its construction and analysis can be extended to other EOS forms or experimental measurements. The application to copper can be straightforwardly reproduced for other crystalline solids, such as iron, aluminum, nickel, silver, etc., and other atomic lattices as well. It can be extended to lattice metamaterials containing links or bars as physical bonds, which can be exactly described by the short-range singum model.

(2) The singum model shows that the binding potential energy described by an EOS is related to the interatomic potential as well, which is given by the singum potential. The simple formulation can provide the fundamental relationship between the elastic moduli and atomic interaction. The pressure- and temperature-dependent elasticity can be derived by the relationship between bond length λ and pressure or temperature.

(3) Although the Vinet EOS was claimed to be universal and indeed exhibits high accuracy in engineering applications, it has limitations to the range of bond length, particularly in high pressures. Therefore, the use of the Vinet EOS imposes a constraint of the effective bond length of the interatomic potential, which is different from the classic interatomic potential, such as the LJ potential or Morse potential.[40] The MB EOS provides desirable flexibility to fit the experimental data and exhibit versatile capability to predict the thermoelastic behavior of cubic crystals.

(4) The singum model does not take into account of the long-range atomic interactions directly. A reasonable hypothesis is that the short-range interaction that occurs between the closest neighbor atoms in the solid bond-length range dominates the elastic behavior, and the long-range interactions produce secondary contribution to the effective mechanical behavior. Assuming its interactional force proportional to pressure, the singum model can fit the experimental data very well for both single crystalline and polycrystalline copper, although different values of parameter s are used.

(5) When only the short-range atomic interaction is considered, one ideal equilibrium state under the zero external pressure condition is the bond length equal to λ at the very bottom of the potential well, which makes $V_\lambda = 0$. However, the actual bond length is shifted from the position, which can be caused by the long-range interaction and be balanced by surface energy as well.[3] When $V_\lambda = 0$, the Poisson's ratio of the solid becomes 0.25, which exhibits some historic meaning and mathematical convenience.[19,57,58]

(6) The singum model considers the effect of surface energy on the elastic behavior through a prestress. It provides an approach to investigate the grain formation of a single crystal. In a finite volume of a lattice, the surface atoms can be the member atoms of singums close to the boundary but cannot form a singum particle as no member atoms exist beyond the surface. Although the inner atoms or singums can reach equilibrium due to the symmetry of the short-range interaction forces, on the boundary layer, the atoms may not stay equilibrium unless the bond length of the atoms on the surface is different from the one for the inner atoms. For example, if the prestress of a crystalline copper at the ambient condition is a positive pressure as a ductile material, which makes the bond

length of singum shorter than the zero force bond length. The repulsive force from inner atoms will push a surface atom away, which requires the neighboring surface atoms pulling it back for equilibrium. Therefore, the surface bond length will have to be larger than the zero-force bond length, which make the surface atom distribution sparser than the inner atoms. Through the difference between the surface bond length and inner bond length as well as the bond angle change caused by the equilibrium, we can estimate the curvature of the surface and then predict the grain size.

(7) Although EOS has been obtained by the experiments of positive pressure and typically exhibits increasing elastic constants with the pressure, the function predicts zero or negative bulk modulus for a certain point at $\lambda > 1$. It may exhibit some physical meaning that the solid state of crystal may start to destruct at a certain bond length, which can be corresponding to either the phase change or melting point. Although it is difficult to validate it by experiments, the singum model can be a useful tool to predict the pressure-dependent melting point or phase change.

(8) When a cubic crystal is subjected to a uniaxial load, the cubic lattice will be tetragonal or orthorhombic. The singum model can be extended to predict the anisotropic elastic behavior. Because the bond length change will be different from different orientations, we cannot restrict the bond length to the shortest one anymore. An ergodic process shall be needed to accurately predict the uniaxal loading behavior. If the critical bond length can be introduced to characterize the load capacity, the singum model can be used to analyze the dislocation and fracture of the crystals. The prestress is related to the surface energy and fracture toughness, which shall be further investigated in future work.

(9) The singum model predicts nonlinear elastic behavior of a lattice in terms of the potential function and lattice parameters using the periodicity of the microstructure. When the lattice structure is subjected to slips, fractures, or other defects, the homogenization mechanism can also be extended to a lattice with a nonuniform effective stress field. The singum stress and strain can be calculated by the same way. Therefore, the singum model can still be used to relate the interacting forces between nodes to the stresses and evaluate the effects of the defects or disorder on lattice structure change and bond breakage. The interatomic forces redistribute with defect formation and change with grain size and boundaries, which can be evaluated by a two-scale modeling with singum strain and stress.

(10) The singum model can be extended to other types of lattices, such as 2D and 3D hexagonal lattices, many-body interaction by adding moment and shear force between the singum's neighbors, or dynamic elastic problems by adding the body force effect as $x_i b_j$ into Eq. (4) where b_j is the inertia force.

Overall, although there are some mature methods to predict elasticity from the interatomic potentials by numerical or analytical methods in the literature, such as EAM,[3] canonical ensemble average with Cauchy–Born rule,[12] and energy equivalence,[2] they derived the stress–strain relationship under the statistical equilibrium condition that does not consider the effect of surface energy, such as surface tension, which produces a configurational force under a displacement variation, and significantly changes the effective elastic behavior. Because the singum model directly links the interatomic force with stress and strain, it handles the surface stress as a prestress. When the prestress is zero, the singum model does recover those old paradoxes of $\nu = 0.25$ for isotropic elasticity and $c_{12} = c_{44}$ for cubic symmetric elasticity. The prestress and the approximation of the long-range atomic interaction successfully addresses these problems and can fit experimental results very well. The exactness of the singum model with short-range atomic interactions can be demonstrated by the granular lattice with the same lattice structure.

VI. CONCLUSIONS

Inspired by granular lattices, the singum model has been extended for the prediction of thermoelastic behavior of cubic crystals. Although the EOS only guarantees high accuracy of $p - \nu$ curves in a certain bond length range, it is sufficient for most engineering stress analysis. Using copper as an example, the singum model provides reasonable agreement with the experimental data for the pressure–temperature-dependent elastic constants. The singum model provides a practical and straightforward way to correlate EOS, interatomic potential, and elastic constants given the lattice configuration. Some interesting features are highlighted as follows:

(1) The thermal expansion coefficient of copper granular lattice can be tailored by the prestress, and copper balls of zero thermal expansion coefficient can be achieved by a copper shell containing copper particles.

(2) When only short-range interactions are considered, when $\lambda = 1$, the polycrystal exhibit a Poisson's ratio $\nu = 0.25$; when $\lambda < 1$, $\nu > 0.25$ and the material is more ductile; and vice versa.

(3) When only short-range interactions are considered, the three cubic elastic constants are not fully independent but satisfy one identity for each type of cubic symmetry.

(4) When long-range interactions are considered, ν varies with the long-range interaction parameter s as well, so it may not be at 0.25 for $\lambda = 1$.

(5) Cauchy discrepancy of $c_{12} - c_{44} = 0$ only occurs at $\lambda = 1$ with short-range interaction. When a prestress and long-range atomic interactions are considered, a Cauchy pressure can be observed.[12]

(6) Using the relation between the bond length change with pressure and temperature, the pressure and temperature derivatives of the elasticity can be analytically obtained with very good agreement with the experiments.

Generally, the singum model interprets the fundamental mechanics and physics of cubic crystals and can be extended to other types of lattices. Although currently it focuses on the static problem with periodic lattice structures, the extensions to general microstructure and dynamic behavior are under way. Particularly, the present model provides a useful tool for material design and analysis under different temperatures and pressures.

SUPPLEMENTARY MATERIAL

The supplementary material is provided to apply the present method to other crystal lattices to verify the singum model. Because the Murnaghan–Birch (MB) equation of state (EOS) shows higher accuracy than the Vinet EOS, the singum potential is formulated with the MB EOS only. Nickel (Ni) and tungsten (W) are demonstrated for face-centered cubic (FCC) and body-centered cubic (BCC) lattices, respectively.

ACKNOWLEDGMENTS

This work was sponsored by the National Science Foundation Nos. IIP #1738802, IIP #1941244, and CMMI #1762891 and the U.S. Department of Agriculture No. NIFA #2021-67021-34201, whose support is gratefully acknowledged.

AUTHOR DECLARATIONS

Conflict of Interest

The authors have no conflicts to disclose.

Author Contributions

Byung-Wook Kim: Data curation (equal); Formal analysis (equal); Investigation (equal); Methodology (equal); Validation (equal); Visualization (equal); Writing – original draft (equal); Writing – review & editing (equal). **Chao Liu:** Data curation (equal); Methodology (equal); Validation (equal); Visualization (equal); Writing – review & editing (equal). **Huiming Yin:** Conceptualization (equal); Formal analysis (equal); Funding acquisition (equal); Investigation (equal); Methodology (equal); Project administration (equal); Supervision (equal); Writing – original draft (equal); Writing – review & editing (equal).

DATA AVAILABILITY

The data that support the findings of this study are available from the corresponding author upon reasonable request.

REFERENCES

[1]K. Fuchs, "A quantum mechanical calculation of the elastic constants of monovalent metals," Proc. R. Soc. Lond. Ser. A Math. Phys. Sci. **153**(880), 622–639 (1936).
[2]R. Johnson, "Relationship between two-body interatomic potentials in a lattice model and elastic constants," Phys. Rev. B **6**(6), 2094 (1972).
[3]M. S. Daw and M. I. Baskes, "Embedded-atom method: Derivation and application to impurities, surfaces, and other defects in metals," Phys. Rev. B **29**(12), 6443 (1984).
[4]P. Vinet, J. H. Rose, J. Ferrante, and J. R. Smith, "Universal features of the equation of state of solids," J. Phys.: Condens. Matter. **1**(11), 1941 (1989).
[5]R. E. Cohen, O. Gulseren, and R. J. Hemley, "Accuracy of equation-of-state formulations," Am. Mineral. **85**(2), 338–344 (2000).
[6]J. Thomas, "Failure of the cauchy relation in cubic metals," Scr. Metall. **5**(9), 787–790 (1971).
[7]J. Martin, "Many-body forces in metals and the brugger elastic constants," J. Phys. C: Solid State Phys. **8**(18), 2837 (1975).
[8]M. Shukla, "Comment on "relationship between two-body interatomic potentials in a lattice model and elastic constants"," Phys. Rev. B **23**(10), 5615 (1981).
[9]A. C. Li, B. Li, R. E. Rudd, and M. A. Meyers, "Dislocation generation in diamond under extreme loading," Matter **6**, 1–17 (2023).
[10]P. Li, Y. Han, X. Zhou, Z. Fan, S. Xu, K. Cao, F. Meng, L. Gao, J. Song, H. Zhang, and Y. Lu, "Thermal effect and rayleigh instability of ultrathin 4h hexagonal gold nanoribbons," Matter **2**, 658–665 (2020).
[11]T.-H. Yang and D. Qin, "Capturing the equilibration pathway of nanomaterials metastable in both crystal structure and morphology," Matter **2**, 519–525 (2020).
[12]E. B. Tadmor and R. E. Miller, *Modeling Materials: Continuum, Atomistic and Multiscale Techniques* (Cambridge University Press, 2011).
[13]Z. Liu, L. Zhang, F. Chongyang, C. Zeng, X. Wu, W. Li, and X. Ma, "Structural, mechanical, and thermodynamic properties of ni-ti intermetallic compounds: First-principle calculation," J. Appl. Phys. **134**(8), 085107 (2023).
[14]H. Chen, D. Liu, and D. Liu, "A computational framework for modeling thermoelastic behavior of cubic crystals," J. Appl. Phys. **133**(3), 035107 (2023).
[15]I. Johnston, G. Narsilio, and S. Colls, "Emerging geothermal energy technologies," KSCE J. Civil Eng. **15**(4), 643–653 (2011).
[16]H. Yin, M. Zadshir, and F. Pao, *Building Integrated Photovoltaic Thermal Systems: Fundamentals, Designs and Applications* (Elsevier, 2021).
[17]C. Liu and H. Yin, "Tailorable thermoelasticity of cubic lattice-based cellular and granular materials by prestress," Mater. Des. **233**, 112223 (2023).
[18]M. Zadshir, C. Liu, J. Lou, and H. Yin, "Advanced material and structural design of a lightweight stiff mounting system for a 50 kw-class photovoltaic array," Technical Report, PVT Clearn Energy LLC, NASA SBIR Phase I, Final Report, Award#: 80NSSC22PB164 (2023).
[19]H. Yin, "A simplified continuum particle model bridging interatomic potentials and elasticity of solids," J. Eng. Mech. **148**(5), 04022017 (2022).
[20]E. Wigner and F. Seitz, "On the constitution of metallic sodium," Phys. Rev. **43**(10), 804 (1933).
[21]H. Yin, "Anisotropy and asymmetry of the elastic tensor of lattice materials," J. Elasticity **154**, 659–691 (2023).
[22]H. Yin, "Generalization of the singum model for the elasticity prediction of lattice metamaterials and composites," J. Eng. Mech. **149**(5), 04023023 (2023).
[23]H. Yin, "Improved singum model based on finite deformation of crystals with the thermodynamic equation of state," J. Eng. Mech. **149**(4), 04023018 (2023).
[24]F. Birch, "Elasticity and constitution of the earth's interior," J. Geophys. Res. **57**(2), 227–286, https://doi.org/10.1029/JZ057i002p00227 (1952).
[25]H. Yin, L. Sun, and J. Chen, "Magneto-elastic modeling of composites containing chain-structured magnetostrictive particles," J. Mech. Phys. Solids **54**(5), 975–1003 (2006).
[26]H. Yin, G. Paulino, W. Buttlar, and L. Sun, "Micromechanics-based thermoelastic model for functionally graded particulate materials with particle interactions," J. Mech. Phys. Solids **55**(1), 132–160 (2007).
[27]K. L. Johnson and K. L. Johnson, *Contact Mechanics* (Cambridge University Press, 1987).
[28]H. Hertz, *Miscellaneous Papers* (Macmillan, 1896).
[29]J. Horabik and M. Molenda, "Parameters and contact models for dem simulations of agricultural granular materials: A review," Biosyst. Eng. **147**, 206–225 (2016).
[30]G. Kuwabara and K. Kono, "Restitution coefficient in a collision between two spheres," Jpn. J. Appl. Phys. **26**(8R), 1230 (1987).
[31]K. L. Johnson, K. Kendall, and A. Roberts, "Surface energy and the contact of elastic solids," Proc. R. Soc. Lond. A Math. Phys. Sci. **324**(1558), 301–313 (1971).
[32]B. V. Derjaguin, V. M. Muller, and Y. P. Toporov, "Effect of contact deformations on the adhesion of particles," J. Colloid Interface Sci. **53**(2), 314–326 (1975).
[33]G. Adams and M. Nosonovsky, "Contact modeling—Forces," Tribol. Int. **33**(5-6), 431–442 (2000).
[34]T. Mura, *Micromechanics of Defects in Solids* (Springer Netherlands, 1987).
[35]D. Maugis, "Adhesion of spheres: The JKR-DMT transition using a dugdale model," J. Colloid Interface Sci. **150**(1), 243–269 (1992).
[36]T. A. Hahn, "Thermal expansion of copper from 20 to 800 k-standard reference material 736," J. Appl. Phys. **41**(13), 5096–5101 (1970).

[37]H. Yin, F. Pao, M. Zadshir, J. Lou, and C. Liu, "Tailoring thermoelastic constants of cellular and lattice materials with pre-stress for lightweight structures," US patent application 17/935,155 (27 April 2023).
[38]Z.-Y. Yin, P.-Y. Hicher, C. Dano, and Y.-F. Jin, "Modeling mechanical behavior of very coarse granular materials," J. Eng. Mech. **143**(1), C4016006 (2017).
[39]C. Goldenberg and I. Goldhirsch, "Friction enhances elasticity in granular solids," Nature **435**, 188 (2005).
[40]P. M. Morse, "Diatomic molecules according to the wave mechanics. II. vibrational levels," Phys. Rev. **34**(1), 57 (1929).
[41]W. Holzapfel, M. Hartwig, and W. Sievers, "Equations of state for Cu, Ag, and Au for wide ranges in temperature and pressure up to 500 GPa and above," J. Phys. Chem. Ref. Data **30**(2), 515–529 (2001).
[42]P. Vinet, J. Ferrante, J. Smith, and J. Rose, "A universal equation of state for solids," J. Phys. C: Solid State Phys. **19**(20), L467 (1986).
[43]L.-R. Chen and Q.-H. Chen, "The test and comparison of three equations of state for solids," Commun. Theor. Phys. **16**(4), 385 (1991).
[44]X. Wei, B. Fragneaud, C. A. Marianetti, and J. W. Kysar, "Nonlinear elastic behavior of graphene: Ab initio calculations to continuum description," Phys. Rev. B **80**(20), 205407 (2009).
[45]P. Vinet, J. R. Smith, J. Ferrante, and J. H. Rose, "Temperature effects on the universal equation of state of solids," Phys. Rev. B **35**(4), 1945 (1987).
[46]M. Milgram, "The generalized integro-exponential function," Math. Comput. **44**(170), 443–458 (1985).
[47]M. E. Suk and N. R. Aluru, "Water transport through ultrathin graphene," J. Phys. Chem. Lett. **1**(10), 1590–1594 (2010).
[48]J. P. Lu, "Elastic properties of carbon nanotubes and nanoropes," Phys. Rev. Lett. **79**(7), 1297 (1997).
[49]H. Yin, L. Sun, and G. H. Paulino, "Micromechanics-based elastic model for functionally graded materials with particle interactions," Acta Mater. **52**(12), 3535–3543 (2004).
[50]H. Yin and Y. Zhao, *Introduction to the Micromechanics of Composite Materials* (CRC Press, 2016).
[51]V. Juvé, A. Crut, P. Maioli, M. Pellarin, M. Broyer, N. Del Fatti, and F. Vallée, "Probing elasticity at the nanoscale: Terahertz acoustic vibration of small metal nanoparticles," Nano Lett. **10**(5), 1853–1858 (2010).
[52]H. Ledbetter and E. Naimon, "Elastic properties of metals and alloys. II. Copper," J. Phys. Chem. Ref. Data **3**(4), 897–935 (1974).
[53]A. Dewaele, P. Loubeyre, and M. Mezouar, "Equations of state of six metals above 94 GPa," Phys. Rev. B **70**(9), 094112 (2004).
[54]H. M. Ledbetter and R. P. Reed, "Elastic properties of metals and alloys. I. Iron, nickel, and iron-nickel alloys," J. Phys. Chem. Ref. Data **2**(3), 531–618 (1973).
[55]N.-Y. Ko, J.-M. Hwang, and Y.-H. Ko, "Behavior of copper under high pressure: Experimental and theoretical analyses," Curr. Appl. Phys. **31**, 93–98 (2021).
[56]Y. Chang and L. Himmel, "Temperature dependence of the elastic constants of Cu, Ag, and Au above room temperature," J. Appl. Phys. **37**(9), 3567–3572 (1966).
[57]S. Timoshenko, *History of Strength of Materials: With a Brief Account of the History of Theory of Elasticity and Theory of Structures* (Courier Corporation, 1983).
[58]Z. F. Yuan and H. M. Yin, "Elastic Green's functions for a specific graded material with a quadratic variation of elasticity," J. Appl. Mech. **78**(2), 021021 (2011).